University of South-Eastern Norway

Faculty of Technology, Natural Sciences and Maritime Sciences

–

Master's Thesis

Study programme: Master of Science in Micro and Nano Systems Technology

Autumn 2023

Mohammad Mehedy Hasan

Diffractive lens development using 3D Gray-scale lithography of Si.

University of South-Eastern Norway

Faculty of Technology, Natural Sciences and Maritime Sciences

Department of Microsystems.

Raveien 215

NO-3184 Borre, Norway

http://www.usn.no

Summary

Diffractive lens is a valuable choice in various optical applications, as they are light in weight and compact in size making them ideal where size and weight are crucial. This characteristic allows the design for more portable and efficient optical system, which can be made using wafer scale MEMS technology. Silicon is a suitable material for infrared optical applications as it is almost transparent in the 3-14 μm wavelength range.

This study is dedicated to the fabrication of infrared diffractive lenses utilizing maskless 3D grayscale lithography of Si with the objective of achieving etching selectivities of 1 to 2. The investigation explores into the effects of various gases, including SF6, O_2, and CHF3, on Reactive Ion Etching (RIE) and how changes in etching rates demonstrate in silicon (Si) and photoresist (PR) when different gas combinations are used. Achieving selectivities of 1 to 2 involves the use of SF6 and CHF3. Selectivity of 2, synonymous with a 4π phase profile, is realized with the gas composition of SF6 at 3 sccm and CHF3 at 20 sccm. This signifies that the structure of the diffractive lens etches twice as deep into the substrate compared to the PR. Similarly, selectivity of 1, means the diffractive lens structure and the PR structure are of same height and depth, is achieved with SF6 at 3 sccm and CHF3 at 40 sccm.

The study also uncovers different RIE relationships and clarifies the important contributing factors. While previous research in grayscale lithography and RIE etching had a predetermined selectivity of 1, it did not offer comprehensive insights into the unique effects of gases employed in the process. This study explores the generation of diverse structures using a direct write laser (DWL) and various RIE recipes to optimize the selectivity.

Acknowledgements

The primary idea for this thesis stemmed from the Optics course during my 3rd semester, which was taught by my supervisor. I would like to express my gratitude to the university of South-Eastern Norway for offering such an inspiring course and for providing me with the opportunity to expand my research knowledge.

I extend my heartfelt appreciation to my supervisor, Mohammad Nadeem Akram, for his relentless assistance and guidance throughout the entirety of this thesis. His patience, motivation, and support have been instrumental in inspiring my research efforts. His wealth of expertise, knowledge, and experience significantly contributed to the quality of my work.

I am also thankful to all my teachers, lab engineers, and seniors for their generous and help.

I am deeply appreciative of the constant support I have received from my parents. Their confidence, trust, and continuous encouragement played a pivotal role in helping me complete my degree.

Contents

Abbreviations

PR: Photoresist

DOE: Diffractive Optical Elements

DWL: Direct Write Laser

RIE: Reactive Ion Etching

RF: Radio Frequency

ICP: Inductively Coupled Plasma

S: Selectivity

MIBK: Methyl isobutyl Ketone

DRIE: Deep Reactive Ion Etching

NPP: Natural Polypropylene

CW: Clockwise

CCW: Counterclockwise

MEMS: Micro-Electromechanical system

NA: Numerical Aperture

SOI: Silicon on insulator

FZP: Fresnel Zone Plates

DI: Deionized

Rpm: Rotation per minutes

sccm: standard cubic centimeters per minute

1 Introduction

1.1 Diffractive optics and their applications

Although we commonly think of light as traveling in straight lines, it exhibits a phenomenon known as diffraction when encountering obstacles or openings. This form of diffraction occurs when light passes through slits or apertures, which can vary in size relative to the wavelength of the light.

The behaviour of light from a distant source as it passes through a small single slit depends on the size of the aperture relative to the wavelength of the light shows in Figure 1. When the aperture is significantly larger than the wavelength, light propagates in a straight line.

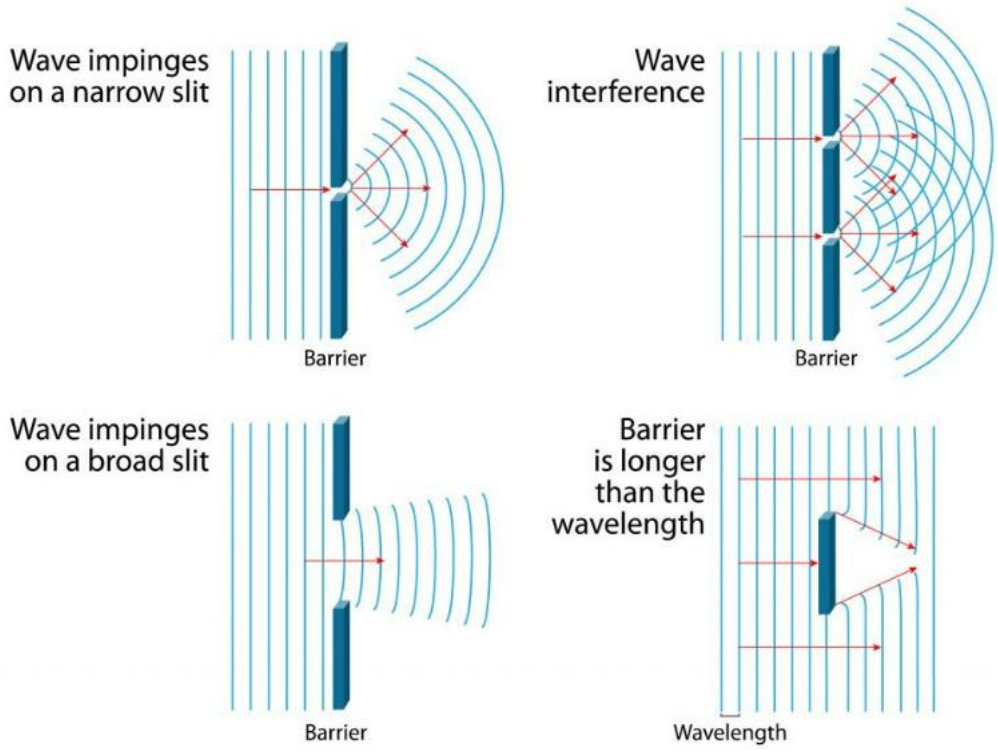

Figure 1 Diffraction of wave when it passes through different slits [1].

However, if the aperture is smaller than the wavelength, and the light comes from a point source, diffraction occurs. This diffraction results in the creation of bright and dark regions,

referred to as maxima and minima. The relationship between the aperture size, wavelength, and the angle of the incident light direction can be expressed using the equation.

$$Sin\ \theta = \frac{\lambda}{d} \quad (1)$$

Here, λ represents the wavelength of the light, d is the aperture size, and θ denotes the angle between the incident light direction and the first minimum of the diffraction pattern [2].

Light exhibits various fundamental properties, including amplitude, phase, direction, and polarization. These properties can be altered by optical phenomena such as refraction, reflection, interference, and diffraction. When interference and phase control are applied, they modify wavefronts through segmentation and redirection, which are characteristics of diffractive elements. A combination of refractive and diffractive elements is employed in many optical components. The smallest spot size achievable at the focal plane is termed the diffraction-limited spot, assuming the lens is free from aberrations. Due to the diffraction at the lens's edges, it is not possible to focus light to a spot smaller than the diffraction-limited spot. In a refractive lens, the majority of the incident light undergoes refraction, while a smaller portion undergoes diffraction. The predominance of either refraction or diffraction depends on the size of the slit opening. If the slit opening is large, the system is primarily controlled by refraction, whereas for a small slit opening, diffraction takes control [3].

There is a fundamental distinction between refraction and diffraction optics. Refractive optics involve the propagation of light in straight lines through a medium with a constant refractive index, and its imaging properties are determined by the refractive index and shape. In contrast, diffractive elements are created by multiple zones, and each aperture contributes to the intensity at a specific spot in the output.

Control of light through diffraction encompasses various techniques, including binary optics, kino-forms, computer-generated holograms, holographic optical elements, and traditional diffraction gratings [4]. These techniques differ in their approach: binary optics provides discrete phase control surfaces, kino-forms offer smooth phase control surface changes, computer-generated holograms are generated by converting interference patterns into

series of phase or amplitude masks, and holographic optical elements are produced by the interference of two wavefronts. The key distinction between holograms and holographic optical elements lies in the complexity of the scenes they can record [4].

When light propagates or bundles of rays pass through optical elements, they form images or create light patterns. To better understand diffractive optical elements (DOE), we should consider wavefronts instead of bundles of rays. Wavefronts are surfaces of oscillating waves, such as light or sound waves, where the phase of the wave remains constant. When light rays arriving from an infinite distance are parallel to each other, and the light rays are perpendicular to the associated wavefronts, these wavefronts are focused by a converging lens with a thicker center and thinner edges. This causes the parallel waves to transform into converging spherical waves with their center at the focal point.

In modern optical systems, hybrid lenses are employed to address aberrations [4]. These hybrid lenses combine traditional refractive elements with diffractive structures on their surfaces as shown in Figure 2. Diffractive structures can effectively correct image and color aberrations when used in conjunction with refractive lenses. Their versatility and ease of design make diffractive lenses valuable tools for lens designers.

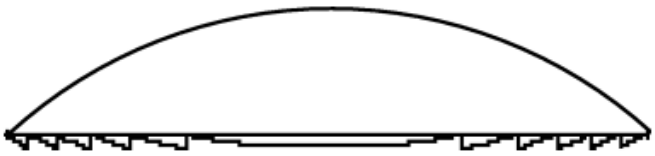

Figure 2 Combination of refractive and diffractive hybrid lens [4]

This thesis explores the creation and optimization of diffractive lenses, delving into the process of their fabrication and fine-tuning to achieve specific lens characteristics.

1.2 Historical Development of Diffractive Lenses

Francesco Maria Grimaldi in 1665 first noticed the diffraction, then Sir Isaac Newton, James Gregory, Thomas Young also continued the research [3].

David Rittenhouse and Joseph von Fraunhofer in the late eighteenth century made significant contributions in diffractive grating. Then many scientists and mathematicians developed diffraction grating and spectroscopic applications. American physicist Henry Augustus Rowland invested Rowland concave grating often referred as Rowland circle spectrometer is an optical device used in spectroscopy to disperse and analyzed different wavelengths of light [4].

Another British scientists Lord Rayleigh made significant contribution in blazed gratings which is a type of diffracting grating that is designed to optimize the diffraction of light at specific angles and wavelengths.

Using Huygens's principle, Augustin-Jean Fresnel explains rectilinear propagation of light and diffraction effect. He made a Fresnel zone plate (FZP) a diffractive optical element which is a circular or annular plate with series of radially alternating transparent and opaque zones [3]. That are used to focus or filter light, sound, or electromagnetic waves. When light passes through a FZP, it undergoes diffraction, leading to constructive and destructive interference. This results in the convergence or focusing of waves at specific distances from the zone plate, similar to how a traditional lens focuses light.

Holography is a technique for recording and reconstructing three-dimensional images invented by Dennis Gabor. He aimed to find a way to capture the complete information about both the amplitude and phase of a wavefront, which was challenging with traditional photographic techniques [3]. Which is accomplished by recording the interference pattern between a reference beam and an object beam of light on a photosensitive medium, typically a photographic plate or film. And hologram is the physical result of the holography process. When the recorded interference pattern is illuminated with coherent light, 3D image can be seen. Hologram produces a 3D image that seems to float in space when an appropriate light source illuminated. The image can be viewed from different angles, and it may exhibit motion or change as the viewing angle or lighting conditions change.

Fresnel lens became prominent in the 20th century which was used to focus or split of the light. These lenses are designed with concentric grooves on their surface which act to diffract or bend the light.

In recent years, diffractive optics have continued to evolve, with advancements in the design and fabrication of diffractive elements. It works by creating phase patterns on the lens's surface to achieve the desired optical effect. Diffractive lenses are often characterized by the presence of micro- or nano-scale structures on their surface, which create diffraction patterns. These patterns interact with incident light to achieve the intended optical function. DOE is used in wide range of applications including laser beam shaping, optical communication and imaging.

1.3 Significance to the field

The development of diffractive lenses through maskless grayscale lithography represents a significant advancement in the field of optics and microfabrication. These lenses offer unparalleled versatility and precision in creating complex three-dimensional structures, which have widespread applications in microelectronics, micro-optics, and fabrication processes. Diffractive lenses provide the capability to engineer and control light in a manner unattainable through traditional binary lithography, enabling the creation of customized optical components with nanometer-level depth control [5]. They open the door to innovations in fields such as telecommunications [4], medical imaging [6], and photonic devices [7]–[12], where customized optical elements are important. This research focuses on the development of Silicon diffractive lenses for infrared imaging and provides insights into fabricating them within various microfabrication processes, allowing the creation of structures at precise depths. This methodology offers the flexibility to manufacture a wide range of structures and lenses adapted to specific requirements.

1.4 Objectives of the research

The primary objective of this research is to develop Si diffractive lenses using maskless grayscale lithography and optimize the entire lens fabrication process. The objectives of this thesis are as follows:

- Develop Si diffractive lenses using maskless grayscale lithography.
- Create complex diffractive lens using maskless laser writer and provide observations into the versatility of the maskless laser writer for diverse microfabrication applications.
- Optimize the entire lens fabrication process and gain insights into optimizing PR coating, PR development, and RIE etching.
- Achieve etching selectivity of 1, refers to achieving an equal etching depth for both the photoresist and substrate, ensuring a consistent and accurate replication of the desired microstructure.
- Utilize two different approaches: test structure and diffractive lens designs to achieve the desired selectivity.
- Focus on understanding the effects of various gases and parameters on the Si and PR in the RIE etching process.
- Investigate potential differences in optimization for different PRs and thicknesses.
- Contribute to the field of diffractive lens development and its applications in microelectronics and micro-optics.

2 Literature review

2.1 Traditional micro-Fabrication Techniques

To design and manufacture a lens there are lots of steps needed to make it. These steps are particularly relevant in microfabrication and the production of diffractive with precise optical patterns as shown in Figure 3.

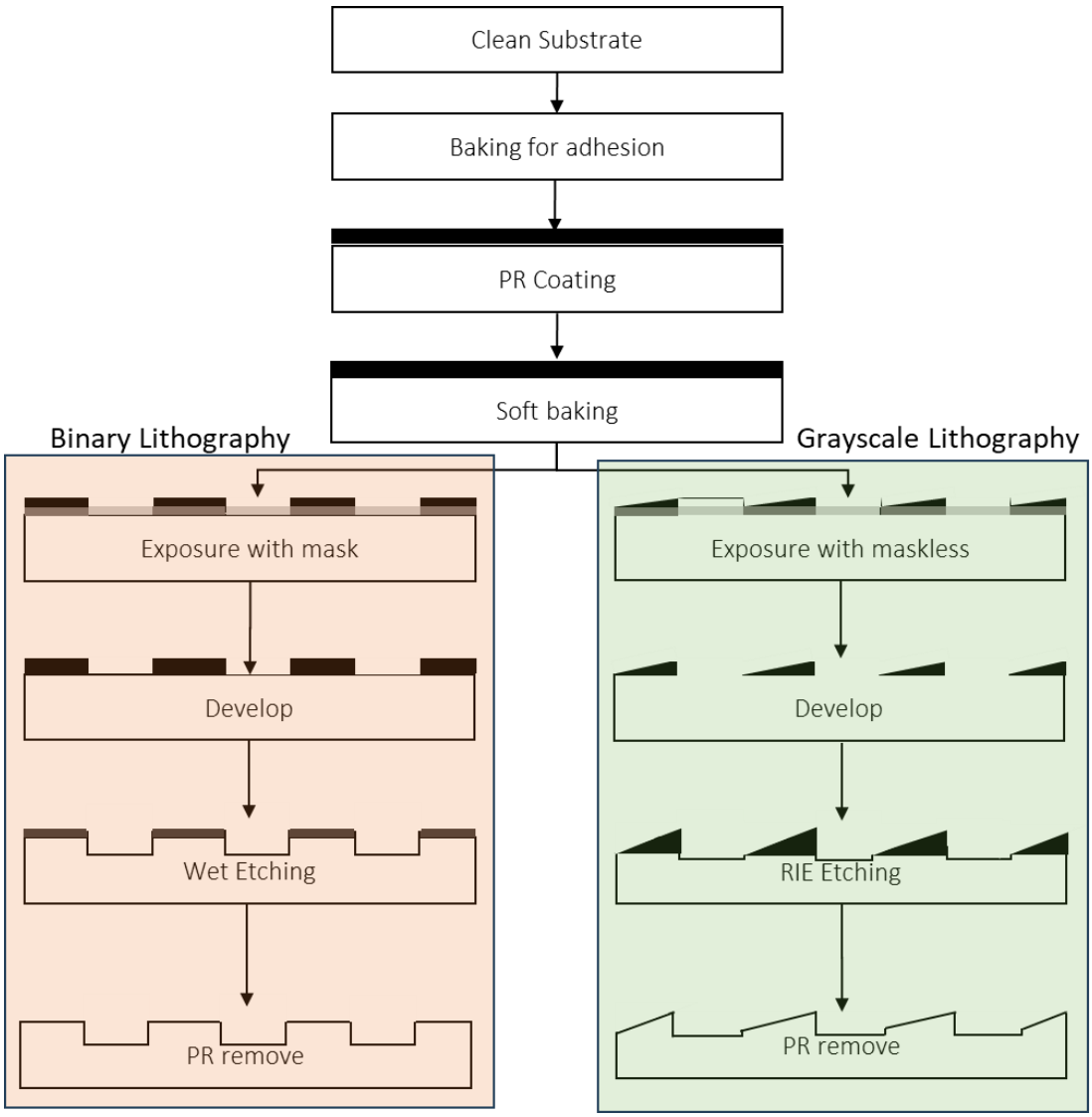

Figure 3 Traditional fabrication process of etching

PRs are used to create extra structure on the substrate surface, this is used as masking material to protect underlying substrate during other processing steps. There are two main

types of PRs: positive and negative PR. Positive PRs are commonly used where the exposed resist dissolves after development. Negative PR behaves opposite when exposed to UV light, negative PR polymerizes and remains after development. Thus, exposed areas become more resistant to developer and unexposed areas are dissolved away during development.

In photolithography process, spin coating is the first process where a thin uniform layer of PR is placed top of the substrate as shown in Figure 4. Liquid PR is spread on the substrate and spin by spinner in a definite time, speed and acceleration for optimal uniformity and thickness. When liquid spreads over the surface of the substrate solvents evaporate.

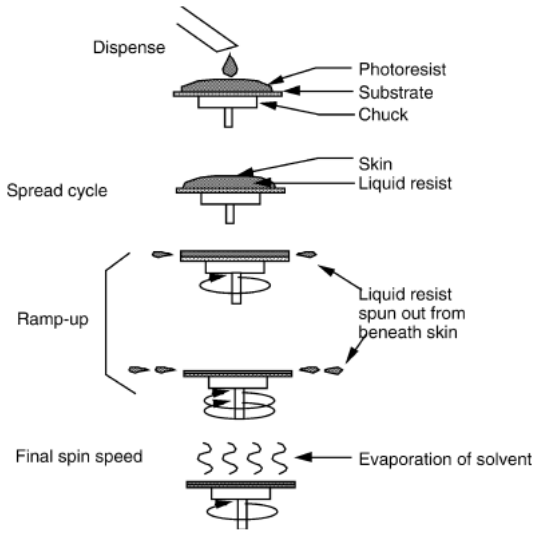

Figure 4 Spin coating process of PR [4]

The thickness of PR layer depends on the combination of viscosity, spin speed, acceleration, and time. To make the PR hard we do the soft baking. This soft baking temperature is not so high, and we keep it for less time in the oven.

Exposure and development process is a key step in photolithography and microfabrication, where a patterned PR layer is used to create precise patterns on a substrate. In this process there are two types of exposure systems: UV exposure with mask and laser exposure without mask.

In UV exposure with mask, where mask can made by glass or plastic which carries the desired pattern, positioned over the PR-coated substrate. Alignment is crucial to ensure that the pattern is accurately placed on the substrate. Then expose the PR-coated substrate to uniform UV light. The photomask acts as a stencil, allowing light to pass through specific patterned areas and block it in others. When UV light is exposed causing chemical change in PR, that's why exposure time and energy is very important. Longer exposure time and higher intensity creates deeper and sharp patterns alternatively less time and intensity cause shallower patterns.

Direct Write Laser (DWL) technique is the laser spot expose without mask in microfabrication and photolithography that is commonly used to design DOE structure. DWL allows for the direct writing of patterns or structures on a substrate without the need for a photomask. Here pattern is design by software program or other design tools and put in the DWL machine and scanning UV laser spot is used to expose the PR-coated substrate. This system typically consists of a focused laser beam, precision motion control, and computer software for pattern generation. Pattern characteristics depend on the laser parameters including laser power, wavelength, exposure time, scanning speed, and the properties of the PR.

After exposure, we immerse the wafer into the developer solution and the developer selectively removes the PR in the areas affected by the exposure. Which area will washed away depends on PR if the PR is positive unexposed areas remain and exposed area will wash away. In negative PRs, the unexposed areas are dissolved, leaving behind the exposed pattern. Here developer time is crucial, if the wafer is developed for longer time, it would damage the pattern, similarly pattern will not be accurate if it is developed for less time.

Etching is a process used in microfabrication and semiconductor manufacturing to selectively remove material from a substrate to create patterns or structures. There are two main types of etching processes: wet etching and dry etching, with reactive-ion etching (RIE) being a common type of dry etching.

Developed wafer with PR is immerse into the liquid etchant solution which is called wet etching because here we use liquid. The etchant chemically reacts with and selectively

removes the exposed material. The etch rate depends on the specific etchant and material properties. Here also, etching time is very important for selectivity. This is an isotropic etching which means etching at equal rates in all directions but some of wet etching also can be anisotropic but it's not common [13].

RIE etching also named dry etching because it doesn't have any liquid. In this process, wafer enters the vacuum chamber and various reactive gases are injected into the chamber and chemically reacts. The selection of materials is influenced by a combination of factors, including their optical characteristics, mechanical attributes, and the level of development in the technology used to process them. RIE etching is usually used in DOE microstructures. RIE techniques are desirable because of highly controlled vertical etching and it is repeatable and well suited for volume manufacturing. This method is preferred in DOE because of its anisotropic characteristics. Anisotropic etching refers to the selective removal of material in a direction perpendicular to the surface, resulting in well-defined and vertical etched features.

In RIE chamber creates plasma by radiofrequency (RF) energy which contain highly reactive ions and radicals. These ions and radicals in the plasma bombard the exposed areas of the substrate, removing material through chemical and physical processes. There are two processes: kinetic and reactive processes. When the wafer is subjected with energetic ions that physically dislodge or sputter material from its surface is called kinetic process. In reactive process chemically reacts with each material [14]. The chemical components in the plasma interact with the molecules in the material being etched, this interaction triggers a reaction that forms volatile gases which means they easily turn into vapor or evaporate, and the etching tool removes them from the material. Ions, which are charged particles, interact with the material on the substrate in a controlled way. This control is achieved by applying a bias voltage that guides these ions towards the substrate with precision. This controlled approach ensures that the ions impact the material in a specific and targeted manner during the etching process. The reactive ion increases the etching rate and higher selectivity. Selectivity and etching rate depend on the material being etched, combination of gases, bias voltage, RF power, pressure, temperature.

After etching, the last process is PR removal which is often used as an etch mask to protect certain areas of the substrate during etching. PR may contain residues or contaminants from the etching process, removing the PR ensures that the substrate is clean and free of any leftover materials or contaminants.

Traditional binary techniques face limitations, notably in their incapacity to generate 3D microstructures and linearly varying depth designs, as opposed to grayscale technology [4]. The traditional method is typically binary lithography, it relies on mask which is restricted to change any design [14]. On the other hand, grayscale lithography emerges as a superior alternative, offering the ability to effortlessly create 3D structures, eliminating the need for masks, allowing for flexible design changes, and facilitating the creation of variant depth structures [4].

2.2 Mask-less Grayscale Lithography as an Emerging Technique

The combination of grayscale lithography and anisotropic etching gives rise to what we call "grayscale technology." Grayscale lithography utilizes variable-dose exposure to control the height and depth of the PR, resulting in the creation of 3D structures after development as shown in Figure 5. Achieving 3D structures can also be done through different methods, such as multi-step exposure [15], direct writing photolithography [16], and grayscale masks [17].

Multi-step lithography involves using several masks, each exposed to varying doses of light, which leads to distinct PR heights for each mask [4]. However, aligning these multiple masks perfectly is a challenging and time-consuming task.

On the other hand, grayscale masks require a unique lithographic mask with a variable transmission profile, and this profile is imprinted into the PR layer. The depth of surface relief in the PR is directly linked to the amount of energy that passes through the corresponding region of the grayscale mask during the development process. By controlled plasma etching or RIE obtained surface relief pattern can be further transferred into the substrate. This approach offers various advantages, notably it eliminates multiple mask alignment thus reducing the fabrication error, time and cost. Nevertheless, it presents certain challenges,

including the intricacy and potentially higher costs associated with mask production. Additionally, the process is notably sensitive due to its dependence on lithographic materials and process parameters.

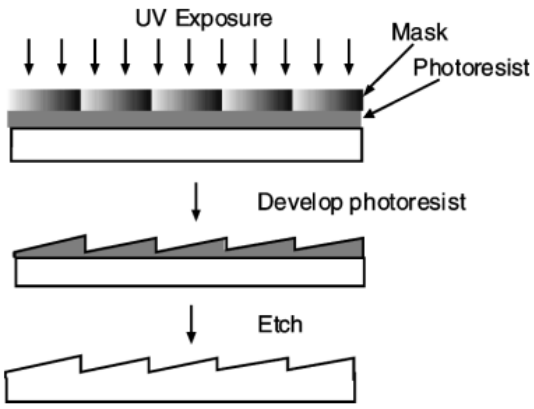

Figure 5 Gray scale lithography with mask [4]

Creating a DOE by directly writing the exposure pattern into the PR using maskless DWL is a widespread practice. Direct writing photolithography which is known as maskless grayscale lithography operates by dynamically adjusting the intensity of the laser writing beam, offering enhanced control and versatility in shaping 3D structures within the PR as shown in Figure 6.

In maskless grayscale lithography, it's essential to experimentally establish the standard sensitivity profile of the PR in use. This is achieved by measuring the height of the developed PR as a function of the local dose applied. There are numerous potential advantages to doing maskless gray scale lithography because this process eliminates lithography mask hence there is no need to make mask, resulting in saving the time and cost. Moreover, it allows for the generation of a large number of phase levels, often ranging from 0 to 256 or even more. It also has one disadvantage: this is a serial process where each element or feature is written or exposed individually, one at a time. This can be a time-consuming process, especially when dealing with complex patterns.

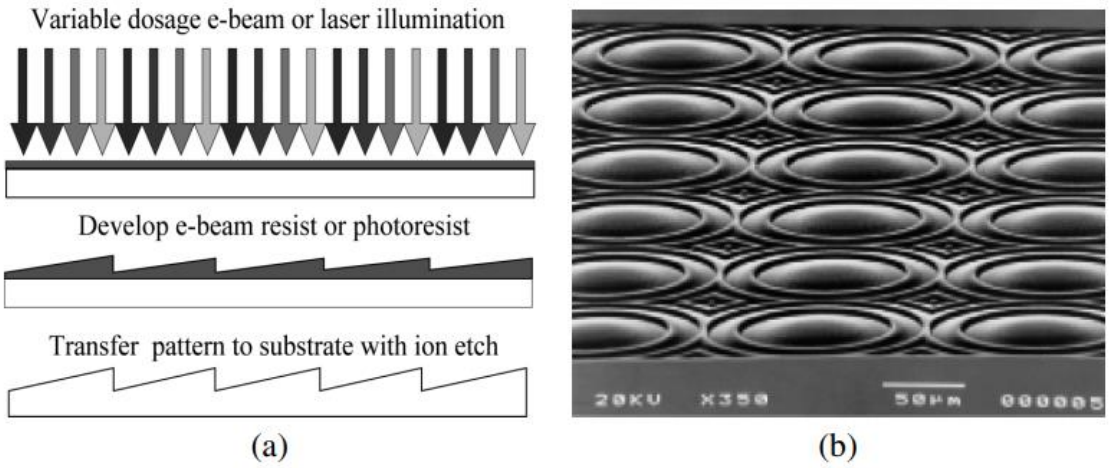

Figure 6 Fabrication method a) Direct write b) Diffractive array lens [4]

After exposure energy, how much PR will remain after development depends on the PR and developer properties. We need to know for a specific PR, what kind of developers are needed, otherwise after exposure PR will not reflect the topographical depth after development.

In this method, etching plays a crucial role in accurately transferring the structure into the substrate. To achieve precision, highly anisotropic etching is required. The term "etch selectivity" (S) refers to the ratio between the depth of the PR and the depth of the substrate after etching. When S equals 1, it signifies that the transferred pattern perfectly matches the PR structure, indicating purely anisotropic equal etching. Conversely, if the selectivity (S) is less than 1, the resulting structure is shallower, while if S is greater than 1, the structure is deeper in substrate as compared to the original PR structure.

Comparing this method and its strengths and weaknesses are presented in below Table 1.

Table 1 Comparison of various method of DOE

Lithography Techniques				
Sl. No.	Lithography method	Materials	Advantage	Disadvantage
1	Binary	Substrate PR Binary mask Developer	Simple method Volume production Surface precision Small feature Very flexible Cost efficient	Limited resolution Loss of information Poor grayscale presentation
2	Grayscale with mask	Substrate PR Grayscale mask Developer	Volume production Analog surface Very flexible	Mask complexity Expensive Process variability
3	Grayscale without mask	Substrate PR Direct laser writer Developer	Analog surface Rapid prototyping Very flexible High resolution gradient Dynamic pattern	Complex data control Low volume Time consuming for large area exposure
4	Grayscale electron beam	Substrate PR Electron beam writer Developer	Analog surface possible Very small feature Very flexible	Complex and costly equipment Slow serial process Limited area coverage

5	Multi-step exposure	Substrate PR Multiple mask Developer	Analog Surface Small feature	Complexity in aligning mask. Mask production error Increased complexity

2.3 Previous Research and Developments

3D structures in crystalline silicon have been achieved through the application of grayscale technology, as outlined in the [18]. This feat is accomplished by employing maskless grayscale lithography and the reactive ion etching (RIE) process. Through a meticulous optimization of the RIE process, a 1:1 selectivity has been achieved, with the anisotropy closely approaching unity. In this case, the PR AZ4562 is used, with a resist thickness of 9 µm, and development is carried out using AZ315B. The RIE etching process employs SF6 at 3 sccm and CHF3 at 35 sccm to achieve selectivity nearing 1. It's noteworthy that in the author's thesis, a similar experiment produced different results, primarily due to the use of a different PR with a thickness of 3.8 µm and a different RIE machine.

In a different study [13] researchers also attained 3D structures with a selectivity of 1, employing grayscale electron beam lithography and RIE. Here, polymethylmethacrylate resist material was used for electron beam lithography, with development in methyl isobutyl ketone (MIBK) resulting in a resist thickness of 100 nm. The desired selectivity close to 1 was achieved through the use of SF6 and O_2 gases, with SF6 introduced at a rate of 45 sccm while varying the flow of O_2. It is important to note that this technique is well-suited for electron beam lithography but not for maskless laser writing, as the results significantly deviated from expectations when similar parameters were applied to the RIE machine.

In another paper [19] researchers employed an 8 µm thick PR, AZ4620, on a silicon substrate. However, the selectivity achieved varied from 0.19 to 2.82, and the gas composition consisted of SF6 at 35 sccm and O_2 at 85 sccm, without the inclusion of CHF3 gas. This study primarily focused on surface smoothness, emphasizing its utility for surface roughness assessment rather than achieving the desired selectivity.

Furthermore, another paper [17] delves into grayscale lithography and Deep Reactive Ion Etching (DRIE). In this research, AZ9245 positive PR was used, with thicknesses of 6 and 7 µm. DRIE etching was employed to transfer the structure into silicon, achieving 2 π and 4 π phase shifts using the Bosch process and relying solely on O_2 and Ar gases. It is worth noting that this process was not well-suited for situations where selectivity was a critical factor, and it lacked detailed information regarding the DRIE etching process parameters.

A separate study [20] explores the use of a high-energy beam-sensitive mask in grayscale lithography to create Fresnel lenses. The PR thickness was 0.6 µm, 1.8 µm, and 5.5 µm, and both RIE etching and DRIE etching were employed to achieve corresponding heights in silicon. Notably, RIE etching was utilized to attain 0.6 µm height, resulting in a selectivity of 0.55. Meanwhile, the DRIE etching process involved CHF3, SF6, and O_2 gases, segmented into three steps: passivation, etch A, etch B, and O_2 plasma. It is important to acknowledge that the application of high-energy beam-sensitive masks can be challenging and costly, which led the author to exclude them from their own research. Nonetheless, this study contributed valuable insights into the etching rates of PR and silicon using various gases and their effects on these materials.

While many papers, such as those cited under [7], [21] discuss DWL using grayscale lithography, they do not provide insights into the RIE etching process or the creation of structures in silicon substrates. Instead, these papers primarily focus on structures within the PR alone. In the paper [7] the authors elaborate on structures in PR using DWL grayscale lithography, utilizing Heidelberg instruments with a laser wavelength of 403 nm and achieving feature heights of 60 µm. Similarly, [21] discusses work with Heidelberg instruments, specifically DWL, employing a positive PR HD8820 with a thickness of 5 µm. In this study, various structures of different sizes, including staircases, pyramids, and nanotechnology buildings, were created. It is noteworthy that these instruments were not employed in my experiments, but these research findings do offer valuable insights into maskless direct laser writing.

2.4 Challenges and Limitations in Existing Research

Since the introduction of grayscale lithography for diffractive optical elements (DOE), various efforts have been made [13] to fabricate and develop structures. In these experiments, electron beam lithography, a complex and costly equipment, was utilized. This study primarily focuses on the combined use of SF6 and O_2, with SF6 held at a constant value, without individual chemical effects being measured.

A thicker PR layer was employed to optimize the creation of a smooth surface structure [17]. The use of higher SF6 and O_2 gases contributed to achieving surface smoothness. However, the addition of CHF3 gas and its potential effects were not discussed. Furthermore, the desired selectivity of 1 was not achieved, indicating that the structure in the PR did not precisely replicate in the Si substrate.

The development of 3D structures and optimization of the reactive ion etching (RIE) process were discussed [18]. Notably, they achieved a selectivity of 1 and close-to-1 anisotropy. This research served as a basis for my own investigations, where it was expanded on RIE optimization. It delved into the varying actions of different chemicals and the combined effects of these chemicals on etching in both PR and Si, each at different ratios. Notably, this aspect was not thoroughly addressed in the referenced research.

3 Methodology

3.1 Equipment and Materials

3.1.1 Spinner SPIN 150i

To produce the PR layer on substrate, a common approach is spinning the PR using spinner, in our case, we used SPIN 150i as shown in Figure 7. This device is designed for precise and uniform coating of substrates with a thin layer of PR material. It typically comprises a rotating chuck, a sophisticated resist dispensing system, and associated control electronics. The chuck securely holds the substrate, often a silicon wafer, and spins it at high speeds while carefully dispensing the PR.

Figure 7 PR spinner POLOS SPIN 150i

The specifications for this equipment are designed to meet a range of coating needs. It can accommodate substrates, including wafers up to 6" (150 mm) in diameter or square substrates up to 4" x 4" (100 mm). Recipe programming is made straightforward through a

user-friendly, large color touchscreen interface, allowing for precise control over the coating process. The equipment features a transparent lid, complete with a syringe holder for central dispensing, providing visibility and convenience during operations. With a chuck speed capable of reaching 12,000 RPM (depending on substrate and chuck type), the equipment delivers high acceleration and accuracy [22]. It also offers the flexibility of manual chemical dispensing and supports both clockwise (CW) and counterclockwise (CCW) rotation. These specifications make this equipment suitable for various coating applications, ensuring precision and versatility in substrate preparation.

3.1.2 Pico-master 150

In this research, we used Pico-master 150i which is a maskless direct laser writer for grayscale lithography as shown in Figure 8. It is a cutting-edge piece of equipment designed for high-precision photolithography and microfabrication processes. It serves as a key tool for creating intricate and customized patterns with exceptional resolution. Unlike traditional mask-based lithography, this instrument directly writes patterns onto substrates without the need for masks. It achieves this by employing a highly focused laser beam to expose PR material. What sets this equipment apart is its ability to control the laser intensity and exposure time at each pixel, enabling the creation of grayscale patterns with varying levels of exposure. This grayscale capability allows for the production of complex, three-dimensional microstructures, including diffractive optical elements and microfluidic devices.

It features a 405 nm GaN laser diode optical module, capable of producing complex structures as small as 300 nm in photo-resist layers, ensuring high-resolution imaging. The user-friendly interface supports both up to 4095 levels of grayscale and pure binary mode, offering exceptional flexibility for customizing patterns, including the creation of 3D optical structures[23]. Real-time laser-controlled auto focus and laser intensity control guarantee the highest quality in imaging.

This laser writer further offers the choice between raster and vector modes, granting a high degree of freedom for designing microstructures in photosensitive layers. It also allows software-controllable selection of write resolutions, facilitating precision in the fabrication

process. The proprietary lightweight objective lens by 4PICO Litho enables real-time auto focus, enhancing accuracy.

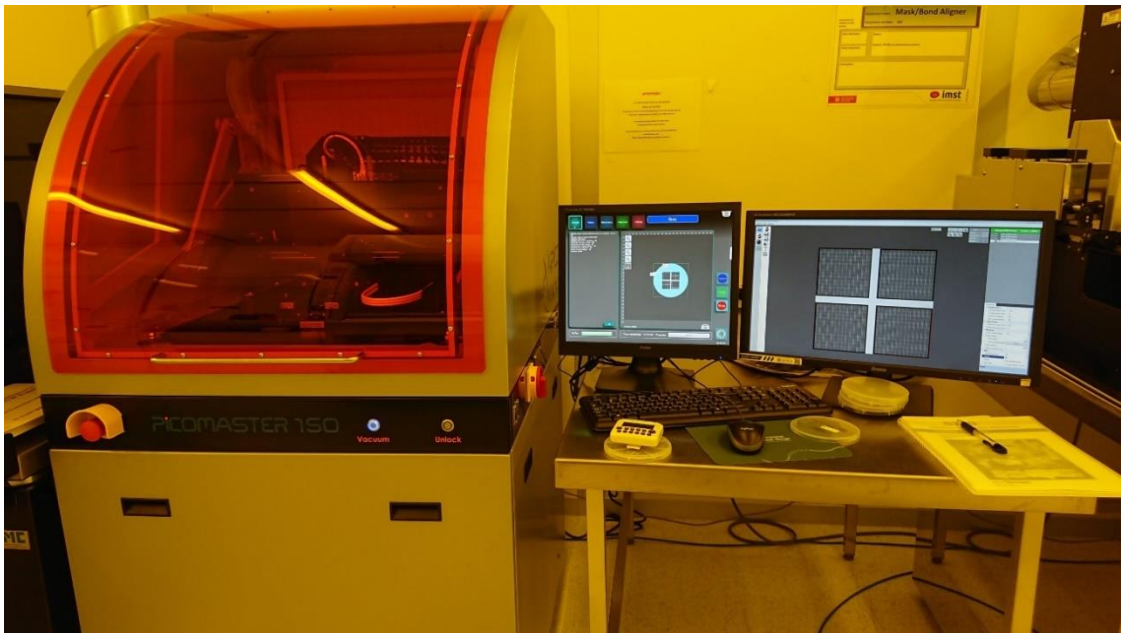

Figure 8 Maskless direct laser writer Pico-Master 150

With support for substrates ranging from 5x5 mm² up to 6"x6" and specifications like a 0.3 µm write mode, a numerical aperture (NA) of 0.85, a working distance of 0.6 mm, and an intensity of up to 3 mW within the spot, this laser writer ensures adaptability to various substrate sizes and the creation of complex microstructures. The pixel resolution of 1 µm, a maximum stroke scan and step of 175 mm, and a scan speed of up to 200 mm/s complete this impressive set of specifications, making it a valuable tool for high-precision microfabrication needs.

3.1.3 Dektak profilometer

Profilometer are used for precise surface profile measurement and characterization across a wide range of industries and applications. It operates by tracing a stylus or optical probe along the surface of a specimen, recording the vertical displacements as it moves. The resulting data is then analyzed to generate highly accurate and detailed surface profiles. One

of the defining features of a profilometer is its versatility, allowing it to measure various types of surfaces, including flat, curved, and irregular ones.

In our experiments we used Dektak profilometer 150 from Veeco as shown in Figure 9.

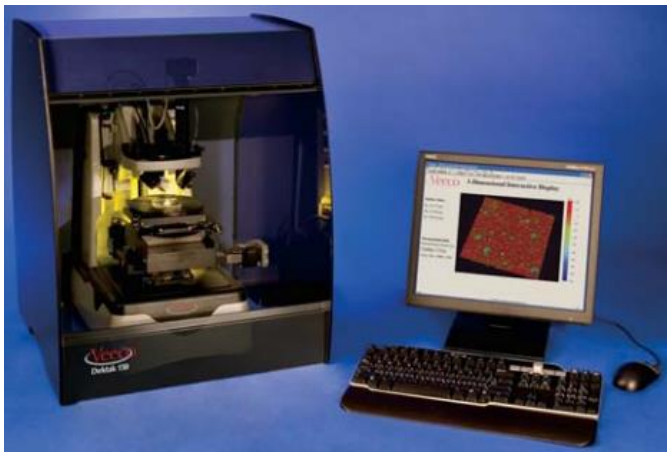

Figure 9 Profilometer DEKTAK 150

This profilometer has an impressive set of specifications, which makes it powerful tools for high-precision surface measurement and analysis. With a standard Z range of 1 millimeter, it accommodates larger step measurements, providing versatility in the types of surfaces it can effectively measure.

The inclusion of the NLite accessory extends its utility to the measurement of soft materials such as PR, enhancing its versatility. The instrument features a length range of 55mm as standard, extendable up to 150mm with the stitching option. It accommodates samples with a maximum thickness of up to 90mm, depending on the configuration.

For wafer measurements, it supports samples up to 150mm, and with the Advanced Automation Package, it extends its capability to 200mm wafers. The instrument excels in step height repeatability, achieving 6Å (D150) with a 4Å option (D150+), making it a top choice for demanding applications. The vertical range of 524µm (1mm optional) provides flexibility in accommodating different sample heights [24].

3.1.4 PlasmaPro 100 Estrelas DRIE

A Reactive Ion Etching (RIE) machine is an important piece of equipment in the field of microfabrication, semiconductor manufacturing, and materials science. This sophisticated device is designed for precise and controlled etching of various materials, offering exceptional versatility and accuracy in the removal of material layers from substrates. RIE machines operate on the principle of chemically reactive gases that, when exposed to radiofrequency (RF) plasma, produce highly reactive ions. These ions, when directed onto the substrate's surface, effectively etch away material, allowing for complex pattern transfer and the creation of microstructures with high precision.

Figure 10 RIE etching machine Plasma Pro 100 Estrelas from Oxford Inst.

Key features of RIE machines typically include the ability to etch a wide range of materials, from semiconductors and metals to dielectrics and polymers. They offer precise control over etching parameters, such as etch rate, selectivity, and anisotropy, allowing for tailored etching processes. The machines may also feature advanced gas handling systems for safe and efficient operation, and some models include multiple gas inlets for custom gas mixtures.

In this experiments PlasmaPro 100 Estrelas DRIE machine is used for dry etching as shown in Figure 10. It boasts high etch rates and excellent selectivity, particularly with the Bosch

process, which ensures efficient material removal while preserving the integrity of the substrate. The result is smooth sidewalls and high aspect ratio processes, enabling the creation of complex and finely detailed structures.

One of its standout features is the ability to produce highly anisotropic (vertical) profiles, making it ideal for applications that require precise and sharply defined etching. It is better in low-rate, low-power etching, making it well-suited for nano-silicon etching and notch control, particularly in Silicon-on-Insulator (SOI) processes [25].

3.1.5 Photoresist (ma-P 1225 G positive photoresist)

Grayscale positive PR is a specialized photosensitive material that plays a pivotal role in advanced photolithography and microfabrication processes. Its primary function is to act as a light-sensitive mask or medium pattern transfer. This unique PR is characterized by its ability to modulate the exposure intensity, allowing for the creation of grayscale patterns with varying levels of light exposure. Unlike traditional binary PRs, which are either fully exposed or unexposed, grayscale positive PR can capture a range of exposure levels, resulting in gradual changes in structure depth or optical density. This versatility makes it particularly well-suited for applications such as diffractive optical elements, micro-lens arrays, and other optical components.

Ma-P 1225 G belongs to the Ma-P 1200 G series. This series of PR exhibits a set of distinctive characteristics tailored for diverse lithographic applications. Notably, it offers reduced contrast, making it suitable for grayscale lithography, where gradual changes in exposure intensity are desired. With the capability to achieve film thicknesses of up to 60 µm and beyond, it enables the creation of deep patterns with a depth range of 50-60 µm. Its spectral sensitivity falls within the range of 350 to 450 nm, allowing for high-intensity laser exposure without concerns of outgassing [26]. The PR is compatible with aqueous alkaline development, making it ideal for grayscale lithography with TMAH-based developers and standard binary lithography using metal ion-bearing developers. It further proves suitable for electroplating processes, dry etch procedures involving gases like CHF3, CF4, and SF6, and

pattern reflow following standard binary lithography, enhancing its versatility for a wide range of advanced microfabrication and nanofabrication applications.

3.1.6 Developer mr-D 526/S

Grayscale developer is a specialized chemical solution used for grayscale positive PRs to create the precise and controlled development of grayscale lithography patterns. Its primary function is to selectively remove exposed regions of the PR, revealing the complex grayscale patterns created during the exposure process. This controlled development process enables the formation of complex, high-resolution structures with varying depths, making grayscale developer an essential component in the production of diffractive optical elements and micro-optics. In this research we used mr-D 526/S developer.

This developer presents good characteristics well-suited for a range of grayscale photolithographic applications. Specifically designed as an aqueous-alkaline-based solution containing surfactants, it is useful for the development of PRs. It offers compatibility with a variety of PR series, including ma-P 1200 and ma-P 1200 G, enhancing its versatility in microfabrication and lithography [27]. This developer accommodates different development methods, including puddle, immersion, and spray techniques, providing flexibility in the development process. Notably, it is suitable for use with PRs from the ma-P 1200 G series, as well as the ma-P 1200 series and ma-P 1275HV, making it an essential component in microelectronics and optics applications, where precise and controlled development of PR patterns is crucial for advanced research and technological advancements.

3.2 Multi-level grayscale design

Diffractive lenses are employed to focus light onto a single point. In comparison to binary Fresnel Zone Plate (FZP), which have limited efficiency of only 40%, diffractive lenses achieve an impressive efficiency of up to 98% [3]. The design and fabrication of these lenses are relatively straightforward [28]–[30], as the phase profile of grayscale FZPs, can be generated using a mathematical equation (2).

$$\left(\sqrt{f^2 + r^2} - f\right) = n\lambda \tag{2}$$

Where f is the focal length of the Lens, λ is the wavelength of the light, r is the radius parameter of the lens.

The phase profile in radians of the Lens is,

$$\varphi(r) = \frac{2\pi}{\lambda}\left(\sqrt{f^2 + r^2} - f\right) \tag{3}$$

Here 2π operation transforms continuous phase pattern of Lens into discrete zones whose phase in between (0, 2 π) radians. The continuous phase profile and discrete wrapped phase profile shows in Figure 11.

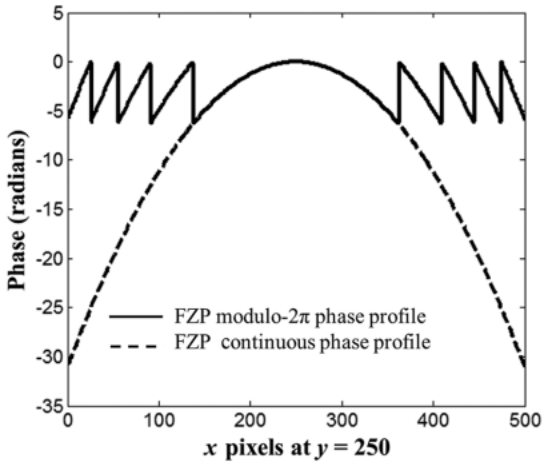

Figure 11 Phase profile of continuous and wrapped.

We design a diffractive lens in MATLAB using the code shown below in Table 2.

Table 2 Matlab code for FZP

```
% FZP, for infinite conjugate
Diameter = 2000; % in um
N=1024; % Matrix size,
dx=Diameter/N; % pixel size in um
f=10000; % Focal length in microns
lambda=10.0; % Wavelength in microns

% Set up matrices,
```

```
% Constructing the FZP Phase
x=(-N/2:N/2-1)*dx; %
y=(-N/2:N/2-1)*dx;
[X,Y]=meshgrid(x,y);
r=sqrt((X).^2+(Y).^2);
A1=-pi/lambda/f*r.^2; % paraxial phase approximation
B=rem(A1,-2*pi);
B(r>Diameter/2)=0;
B=B+2*pi;

% Now normalize this to 0 to 255, and write matrix B as BMP file.
B=B/2/pi;  % Normalize to 1.0;
B= 255*B;  % Normalize to 255;
B = uint8(B); % convert to Integrer values 0 to 255

figure;plot(B(:,N/2));
figure;imagesc(B);axis image;colorbar;colormap gray

% write to BMP file as 8bit format
imwrite(B,'FZP.bmp');
```

Output result of the Matlab code is shown in Figure 12.

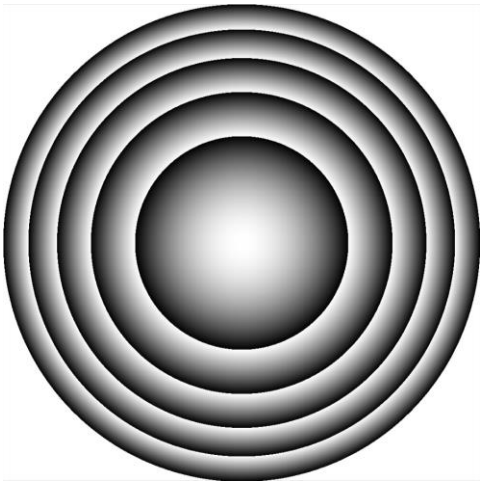

Figure 12 Image of the phase profile of FZP diffractive lens

This code output is made as BMP file because PicoMaster DWL can read only BMP file as the mask.

For this lens, we assume wavelength of incident light is λ = 10 μm.

Height of the grating for 2π phase shift:

$$h_{max} = \frac{\lambda}{n-1} \quad (4)$$

$$h_{max} = \frac{10}{3.417 - 1} = 4.127\ \mu m$$

Where, *n* is the refractive index of Silicon, which is 4.417, so, maximum height of the Si etch can be 4.127 μm. In our experiment we got resist height as 4μm. Diameter of the lens is d= 2,000μm and focal length f= 10,000μm.

3.3 Process Design and Optimization

In this research, pursued two distinct approaches to enhance the lens manufacturing process shown in Figure 13. The first involved a test structure design, where we determined the resist thickness by precisely controlling the spinner's speed and time. Additionally, we identified the precise development time necessary after exposure and optimized the RIE etching process recipe to ascertain etching rates for PR and Si.

The second approach centered around diffractive lens design. In this method, PR thickness was consistent same as the test structure. Using MATLAB, we designed the lens and then transferred the design onto the wafer through a maskless direct laser writer. Following exposure, the lens underwent the same spinning and development time parameters as the test structure. For RIE etching, an optimized recipe was applied to achieve a selectivity of 1, ensuring the production of high-quality diffractive lenses.

In these two processes, all parameters remain consistent until the soft baking step. The divergence begins with the lens exposure phase. After PR development, the depth and condition of the structure are evaluated using both a microscope and a profilometer. If the depth and structural integrity meet the required standards, the process proceeds to the next stage; otherwise, exposure and development must be repeated as shown in below flowchart.

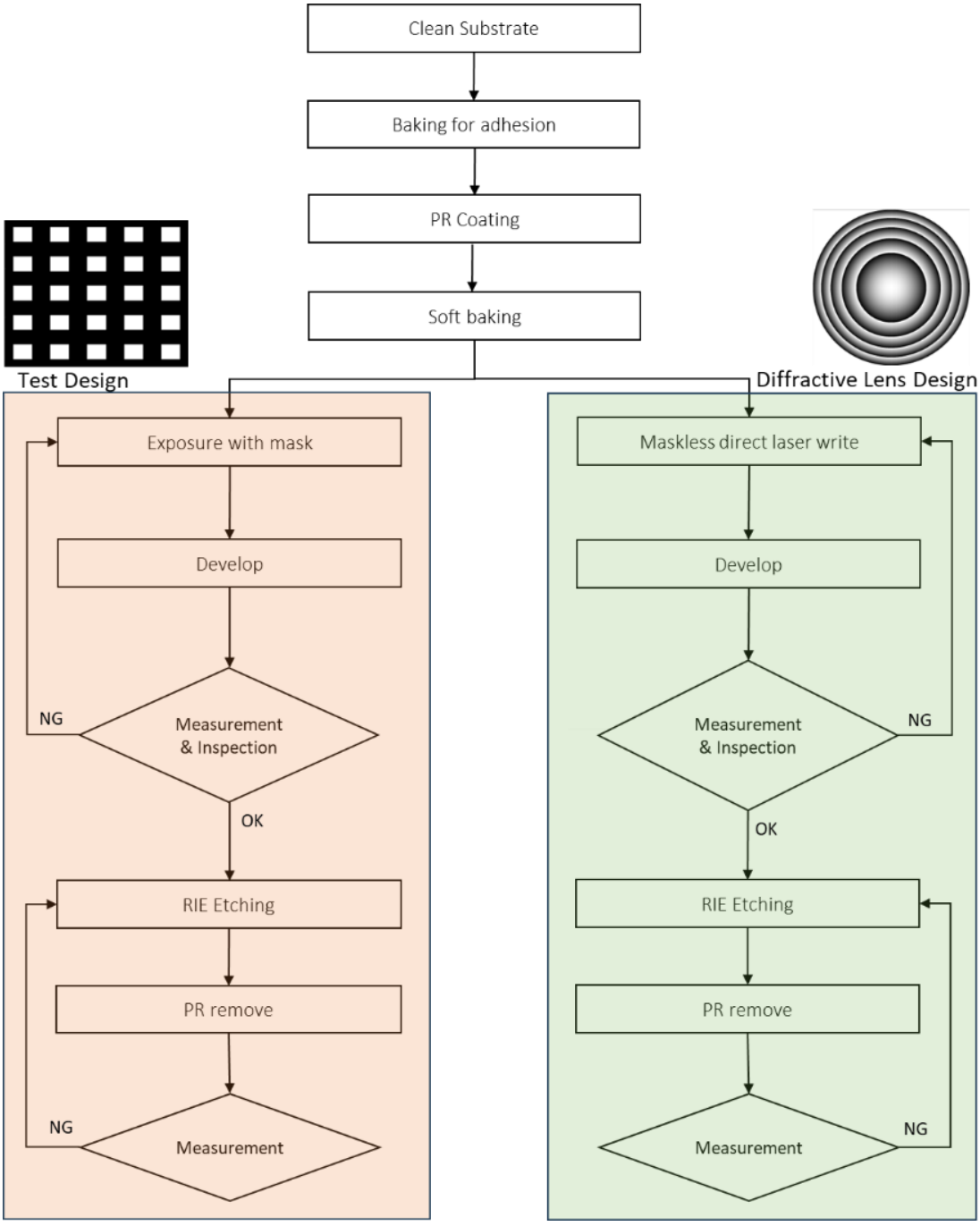

Figure 13 Process flow chart of test structure and diffractive lens fabrication process

Upon completion of the development process, we proceeded with RIE etching, where various gas combinations were systematically employed to fine-tune the process. Throughout this research, we conducted nearly 60 RIE etching iterations using different gas combinations, gaining valuable insights into the diverse effects of these gases on both the substrate and the PR.

3.4 Process description

3.4.1 Wafer preparation

Wafer preparation involves various steps. If the wafer has any dust or dirt, a cleaning process is initiated. In the presence of flying dust, nitrogen gas is employed for cleaning, otherwise we clean the wafer by deionized (DI) water and nitrogen. Subsequently, the wafer undergoes prebaking at a temperature range of 105-110°C for a duration of 5-10 minutes. After this, a final nitrogen blow is administered to eliminate any flying particles, and the wafer is allowed to cool. This controlled heating aids in establishing strong adhesion of the PR. In this research we used ma-P 1225 G positive PR which is efficient for grayscale lithography. This PR is characterized by its thickness and low contrast properties, as elaborated in section 3.1.5. To achieve a desired PR thickness of 4 micrometers, the POLOS 150i spinner is utilized, with specific spin speeds and durations outlined in the Table 3.

Table 3 Relationship between spinner speed and resist thickness

	Spinner			PR thickness (μm)			
Wafer no.	speed (rpm)	Time (sec)	Acceleration (rpm)	Left	Middle	Right	Average
1	1000	35	400	3.64	3.65	3.67	3.65
2	1500	35	400	2.88	2.96	2.92	2.92
3	2000	35	400	2.45	2.52	2.44	2.47
4	2500	35	400	2.15	2.20	2.13	2.16

When the spinner rotates at high speeds, the resist spreads rapidly, resulting in less resist remaining on the wafer. At 2500 rpm, the average thickness is reduced to 2.16, which is nearly half of the thickness achieved at 1000 rpm.

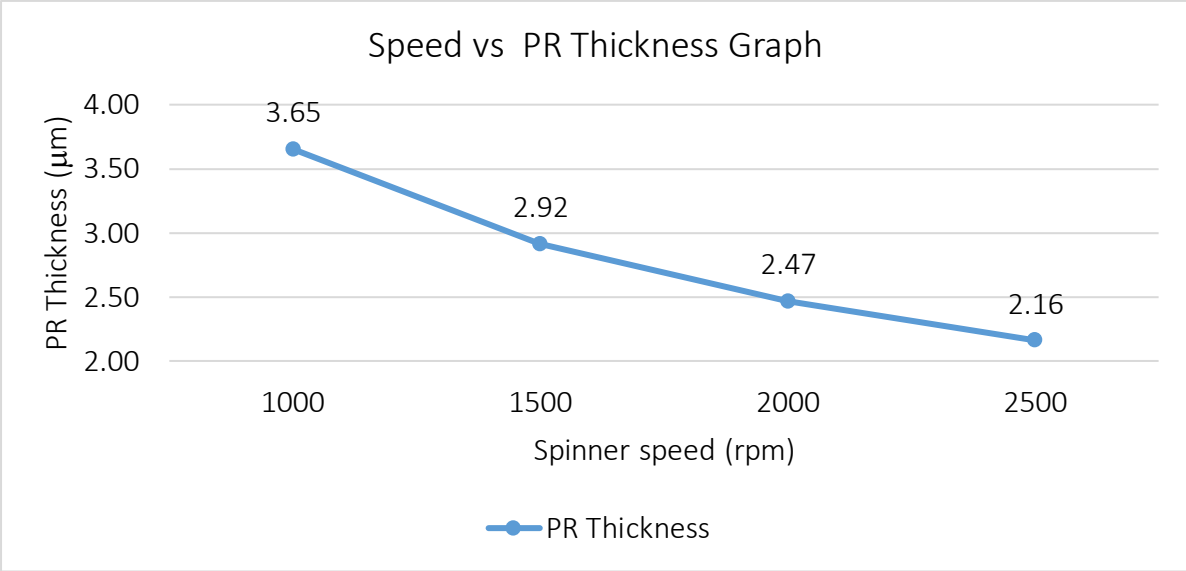

Figure 14 Spinner speed Vs PR thickness graph

We measure the PR (PR) thickness at three distinct points on the wafer: the left side, the middle, and the right side. Calculate the average of these three values. The experimental results reveal an inverse relationship between PR thickness and spinner speed; as spinner speed increases, PR thickness decreases, and conversely, decreased speed results in increased PR thickness as shown in Figure 14. In designing our diffractive lens, the goal was to achieve a PR thickness of approximately 4 micrometers. Based on this data, the spinner's speed was set at 1000 rpm for 35 seconds, with an acceleration of 400 rpm. It's crucial to avoid very low spinner speeds, as it can lead to an uneven PR surface, resulting in non-uniform film thickness and reduced resolution.

Following the spinning process, a soft bake was conducted at 105°C for 50 seconds. PRs typically contain solvents that aid in achieving uniform coating. The soft bake step facilitates solvent evaporation, reducing the risk of air bubbles and expediting PR drying. Soft baking also enhances the adhesion of the PR to the substrate and contributes to uniformity. While

two temperature settings were tested for soft baking (50 seconds and 60 seconds), the 50-second duration yielded superior results, as indicated in the Table 4.

Table 4 PR soft baking and PR thickness

Baking and developing time optimization								
Sample No.	Lens No.	Bake after PR Time (sec)	Laser printing Power (250 mJ/cm^2)		Developing time (s)	Profilometer measurements (um)		
			Power Ratio (%)	Power (mJ/cm^2)		Left	Center	Right
1	1	60	100	250	45	3.3	2.6	2.6
	2		96	240		3.2	2.6	2.6
	3		92	230		3.2	2.5	2.6
	4		88	220		3.1	2.5	2.6
	5		84	210		3.0	2.4	2.6
2	1	50	100	250	45	4.0	3.4	3.3
	2		96	240		3.8	3.3	3.4
	3		92	230		3.7	3.2	3.3
	4		88	220		3.7	3.1	3.2
	5		84	210		3.5	3.1	3.2

3.4.2 Photoresist design and development

3.4.2.1 Test structure design

To facilitate the RIE etching process, two lithographic methods were employed. In order to determine the PR (PR) thickness and comprehend the etching rate during RIE, an initial binary photolithography step was carried out using the Karl Suss MA56 mask aligner. This process not only allowed the measurement of PR thickness but also simplified the evaluation of RIE etching rates of Si.

This is just a binary square pattern mask which create square pattern on the PR as shown in Figure 15. This choice of mask allowed for the exploration of PR thickness, determination of optimal development times post-exposure, and the fine-tuning of the RIE process.

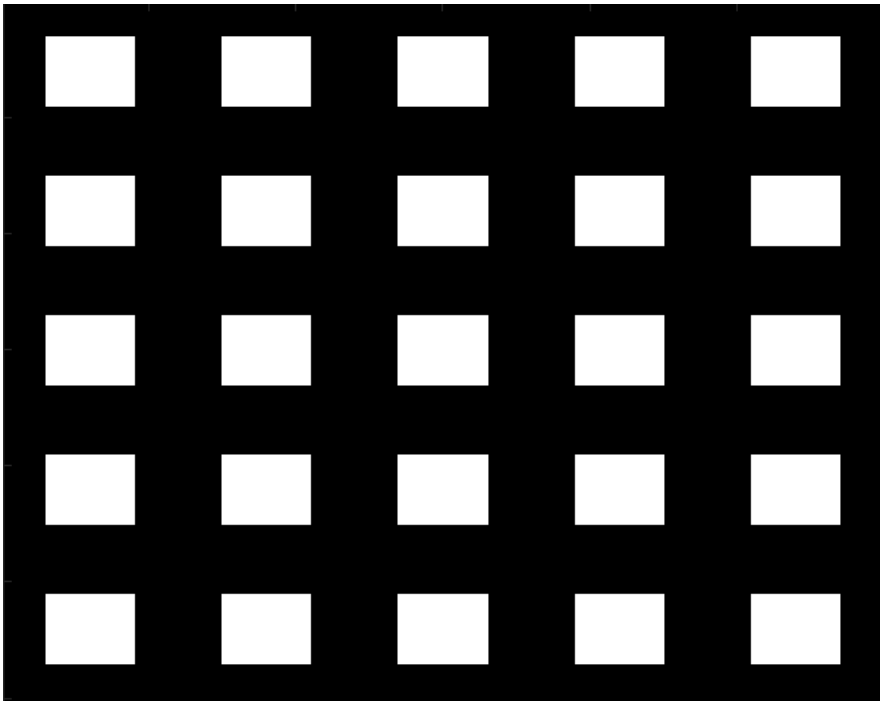

Figure 15 Test structure design

To make a square pattern, we used mask aligner MA56 with parameter details as in Table 5.

Table 5 Mask aligner parameters

Contents	Value
Light intensity (mW/cm^2)	1.22
Exposure time (s)	50
Exposure wavelength (nm)	365-405
Light source (W)	350

Following UV exposure with a mask aligner, the wafer underwent development using developer mr-D 526/S. The development time ranged from 45 to 60 seconds. Notably, in binary pattern development, time flexibility allows for considerable variations. However, when working with grayscale patterns, the development time must be precisely controlled due to its sensitivity. Overdevelopment can harm the structure, while underdevelopment results in inadequate PR removal.

Subsequent to development, we measured the PR thickness using a profilometer (Dektak 150). We successfully attained the targeted PR thickness of nearly 4 μm.

3.4.2.2 Diffractive lens design

To implement diffractive lens, we employed the maskless laser writer Pico Master 150. The process began with the design of the lens using Matlab which is already explain in section 3.2, followed by the creation of a BMP file, as the laser writer's compatibility to BMP format. Subsequently, the BMP file was imported into the PicoMaster project manager. The machine's setup was configured, aligning the BMP file's coding from 0 to 255, thereby modulating power intensity across the entire range. This setup involved the calibration of several parameters, encompassing laser power, energy, target power, exposure dose, with details are in Table 6.

Table 6 Pico-Master 150 laser writer parameter

Contents	Value
Target power	150 μW
Exposure dose	250 mJ/cm^2
Required power	165 μW
Max power	200 μW

We selected the program with a medium-resolution aperture and no reduction attenuator. it's because medium resolution provide balance between speed and resolution, it also allows to create fine details and complex patterns as shown in Figure 16. The power dose intensity was contingent upon the attenuation setting. In the context of laser resolution, both the attenuator and the aperture were configured to medium resolution. Additionally, we had the flexibility to select the laser power percentage, determining the level of power intensity dedicated to generating the entire structure. In the table below, we can see that medium resolution and no reduction provide maximum power intensity of 1600 μW.

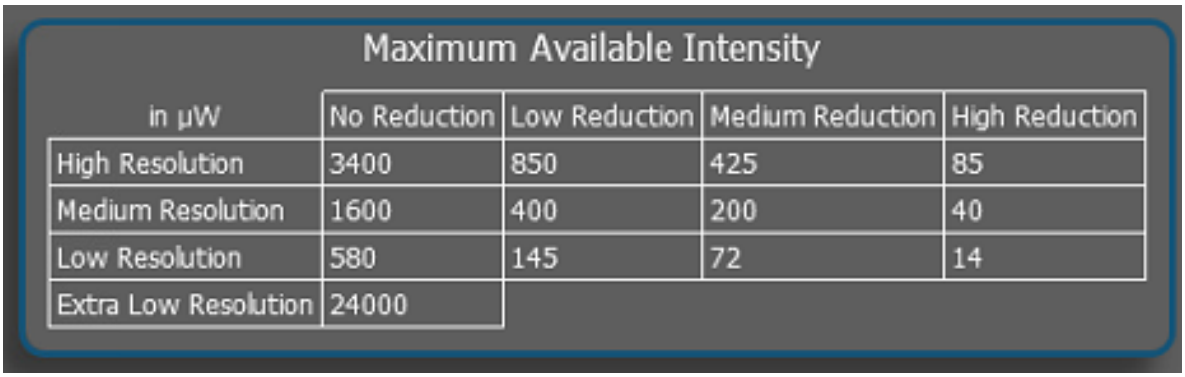

Figure 16 Maximum available intensity w.r.t. resolution and reduction parameters in PicoMaster DWL

We created structures with exposure doses at power setting of 100%, 95%, 90%, 85%, and 80%, subsequently assessing the depth of the PR (PR) as shown in Table 7. These percentages correspond to the exposure dose, with 100% representing the set value of 250 mJ/cm^2, and 95% denoting an exposure dose of 237.5 mJ/cm^2 and so on.

Table 7 Maskless laser writer power dose.

Target power (μW)	Exposure dose (mJ/cm^2)	Exposure intensity percentage	Actual exposure dose (mJ/cm^2)	PR height (μm)
100	250	100%	250.0	3.26
		95%	237.5	3.18
		90%	225.0	3.13
		85%	212.5	3.01
		80%	200.0	2.99

As evident in the Table 7, a reduction in exposure dose corresponds to a decrease in PR height, signifying that lower laser power resulted in reduced etch depth within the PR. The measurement of the lenses was carried out using a profilometer, and the resulting curves are presented in the Error! Reference source not found.Figure 17, Figure 18, Figure 19, Figure 20 and Figure 21 respectively. Notably, there were no considerable differences in the structure itself; the only variation observed referred to the depth of the structure.

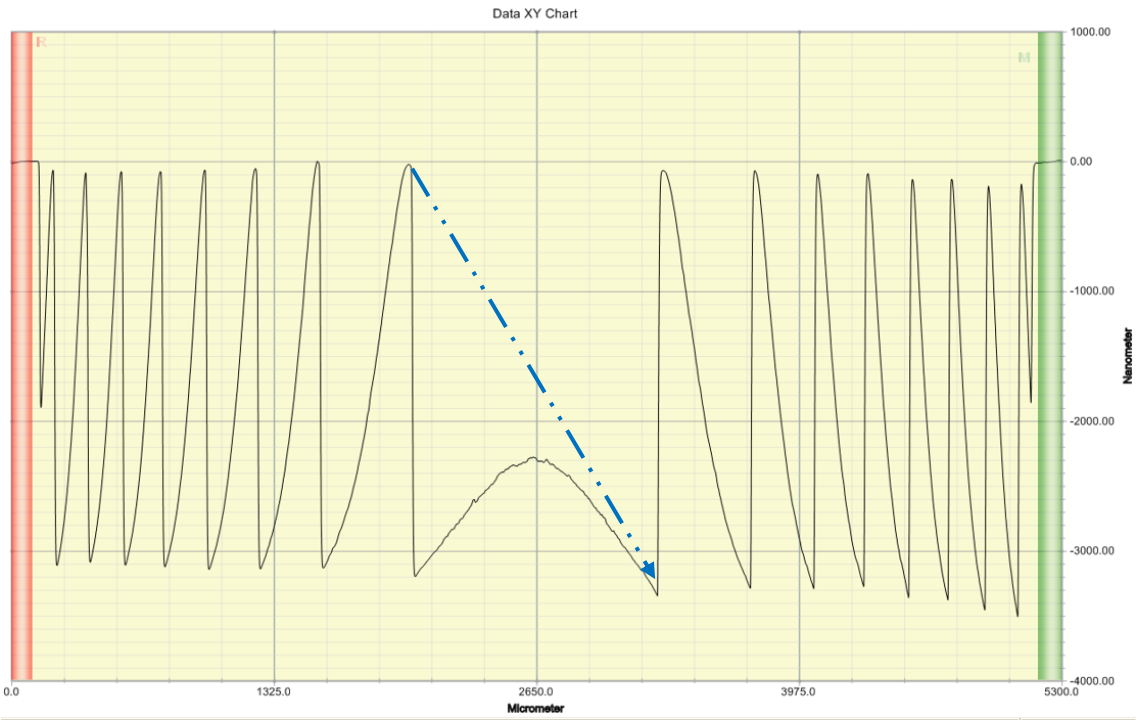

Figure 17 Profilometer data after laser writing at 250 mJ/cm2 where PR depth is 3.26 um as shown in table 7.

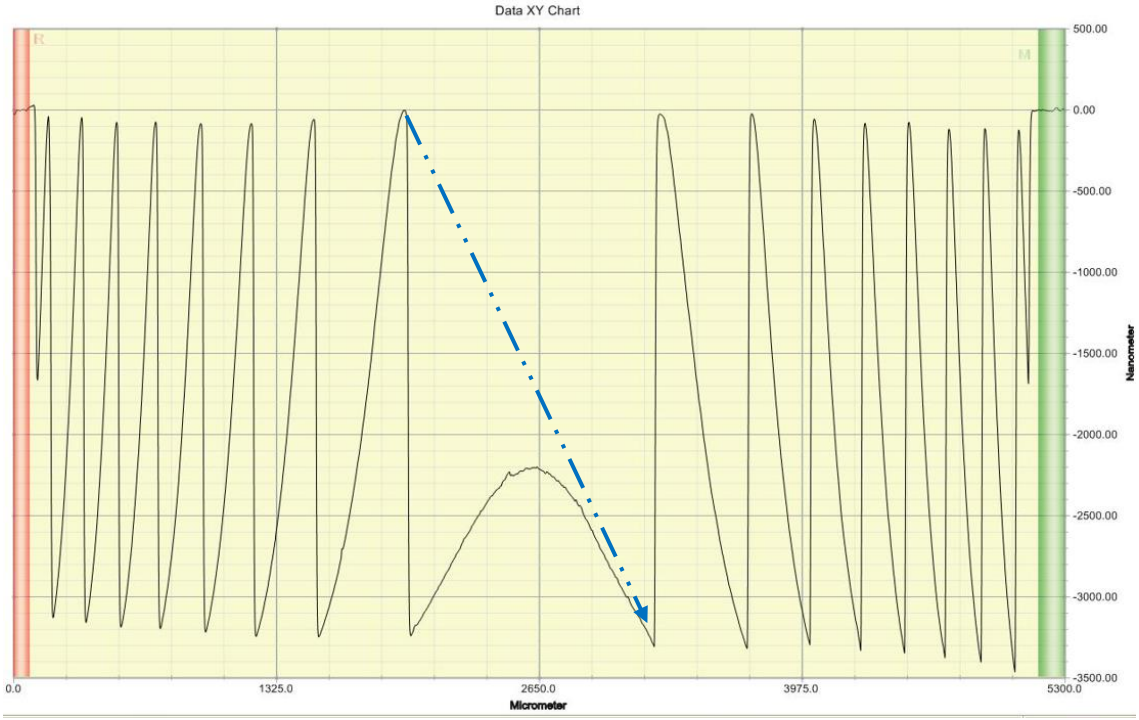

Figure 18 Profilometer data after laser writing at 237.5 mJ/cm2 where PR depth is 3.18 um as shown in table 7.

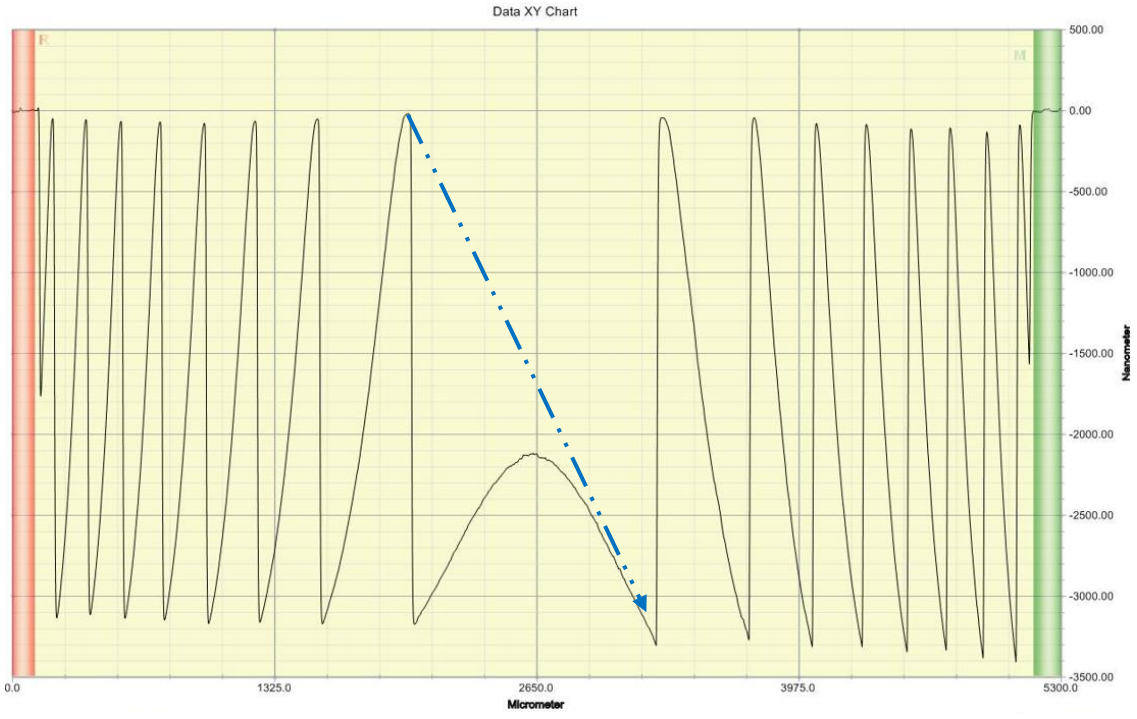

Figure 19 Profilometer data after laser writing at 225 mJ/cm2 where PR depth is 3.13 um as shown in table 7.

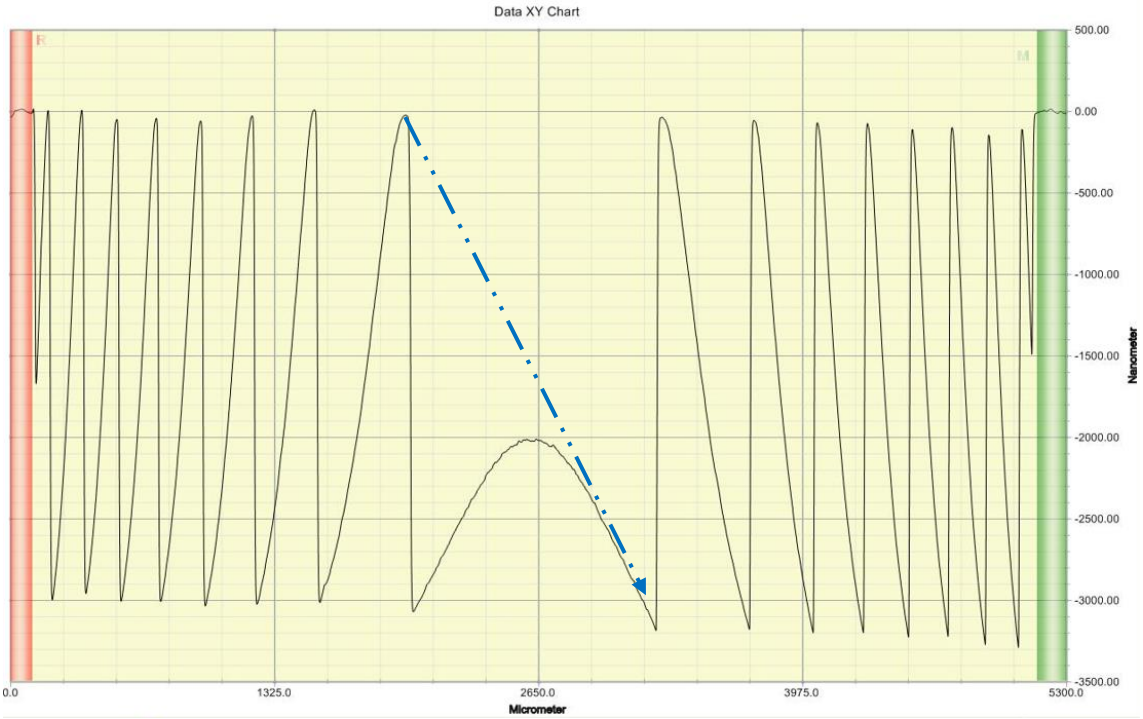

Figure 20 Profilometer data after laser writing at 212.5 mJ/cm2 where PR depth is 3.01 um as shown in table 7.

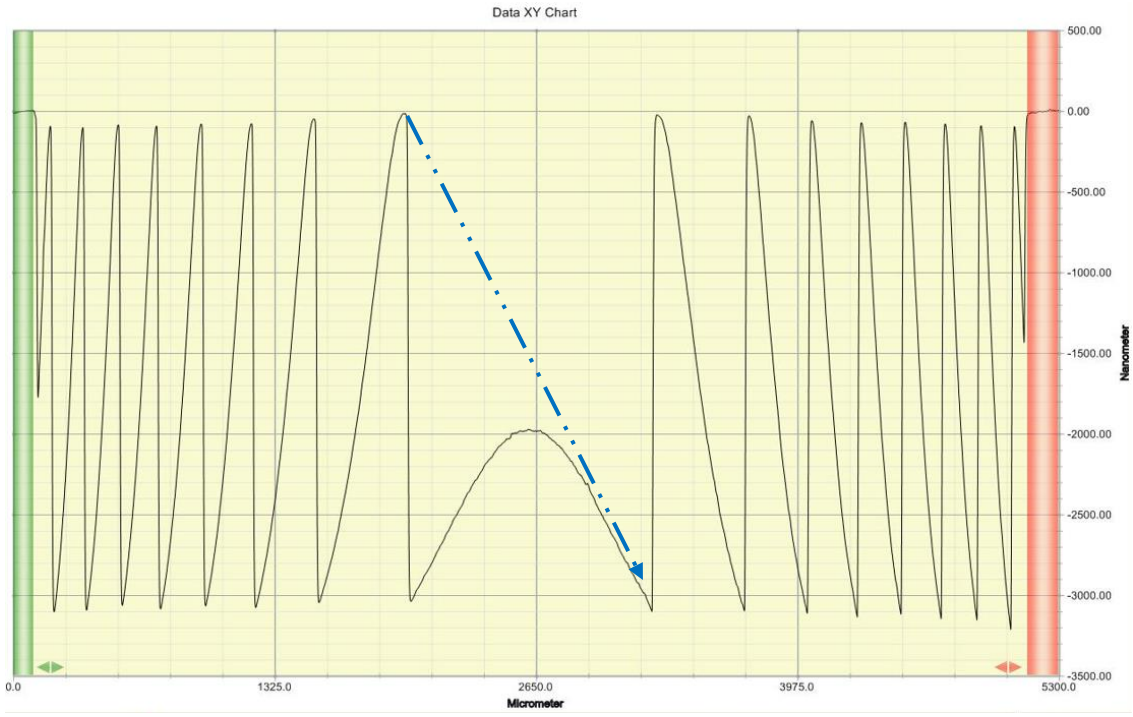

Figure 21 Profilometer data after laser writing at 200 mJ/cm2 where PR depth is 2.99 um as shown in table 7.

To determine the precise depth of the structure, we conducted measurements at four distinct points as shown in Figure 22 and subsequently compared the results obtained from each of these measurements. It's worth noting that the overall area of the lens encompassed a 5 x 5 mm space.

Figure 22 displays the four designated measuring points, and the corresponding measured values are provided in Table 8. The measurements of each power dose exhibit uniformity, and the structures are of high quality.

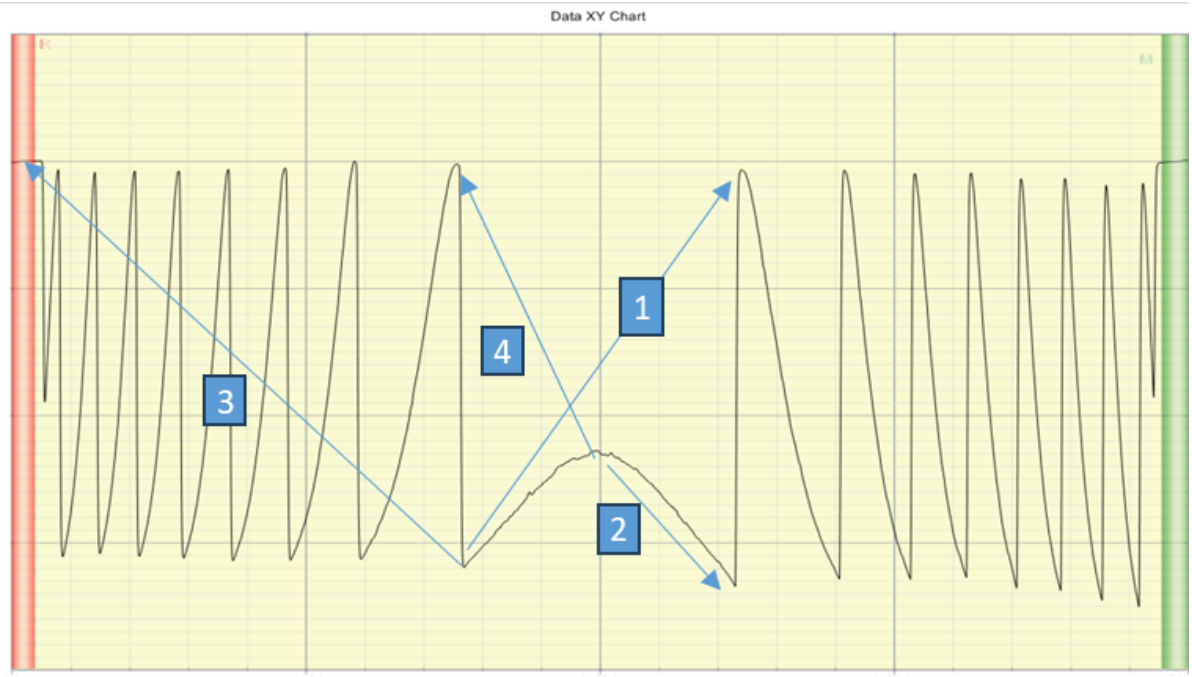

Figure 22 Measuring points in profilometer.

Table 8 Profilometer measurement at various laser power

Depth of PR at different exposure energy					
Exposure intensity	Exposure energy (mJ/cm^2)	Measured value (μm)			
		1	2	3	4
100%	250.0	3.26	0.92	3.32	2.36
95%	237.5	3.18	1.00	3.20	2.20
90%	225.0	3.13	1.06	3.15	2.06
85%	212.5	3.01	1.08	3.05	1.92
80%	200.0	2.99	1.04	3.02	1.95

Across all the measurement points, the 3D structure exhibited consistency. Following this assessment, the wafer underwent development using the mr-D 526/S developer for varying time intervals, specifically at 35, 40, 42, 47, 50, and 60 seconds as shown in Table 9.

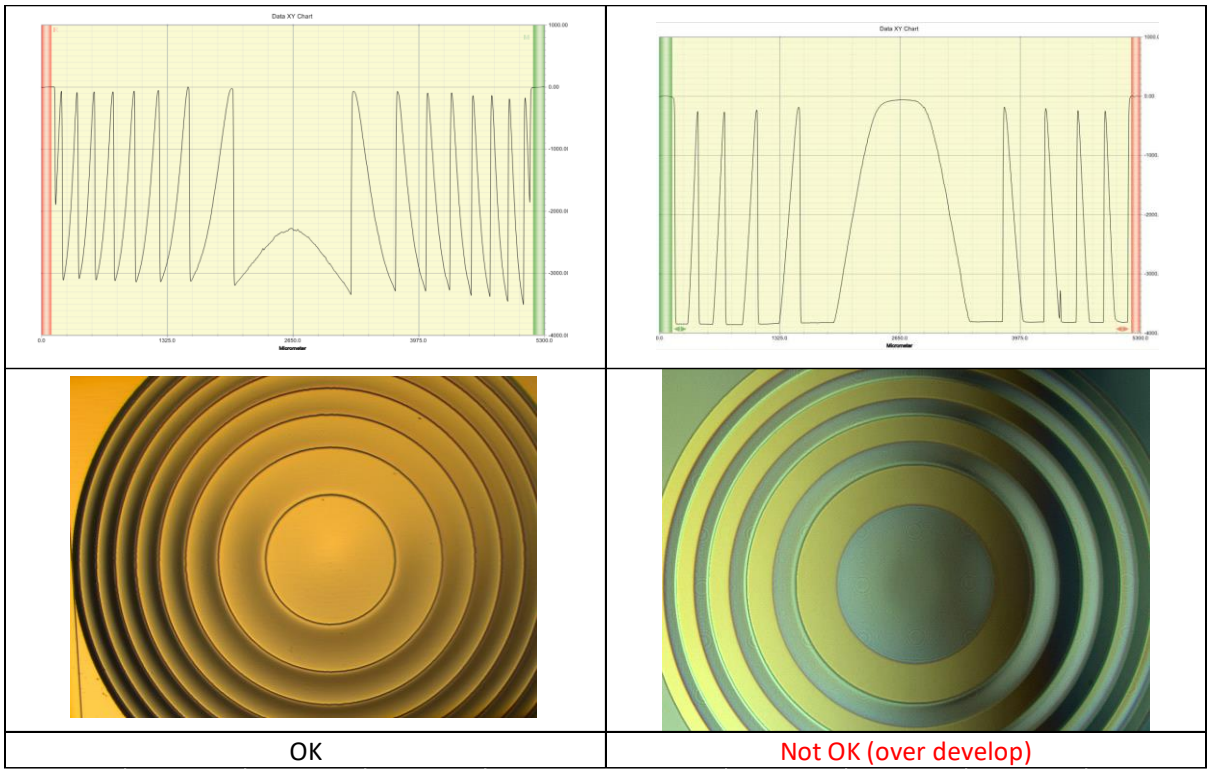

OK	Not OK (over develop)

Figure 23 Diffractive lens normal developed (left) and over developed (right).

Development duration less than 40 sec is proved insufficient for complete PR development, while periods exceeding 50 seconds led to excessive PR removal in grayscale lithography as shown in Figure 23.

Table 9 PR measurement at various development time

Soft baking		Development	Measurement (μm)
Temp (C)	Time (s)	Time (s)	
105	50	35	2.7
		40	3.1
		42	3.2
		45	3.3
		47	3.4

Throughout my research, the wafer development duration ranged between 42 to 46 seconds, although it wasn't a fixed parameter and exhibited variations from one wafer to another. This variation is due to the pattern sizes and small differences in PR thickness across wafers. Additionally, minor variations in baking time and temperature contributed to the small differences in development times among wafers. It was necessary to check the condition of the patterns through a microscope.

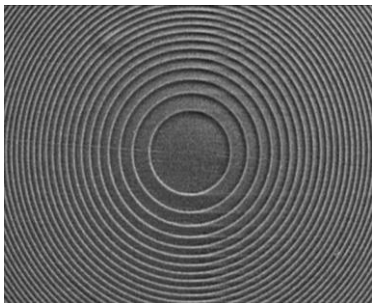

(a)

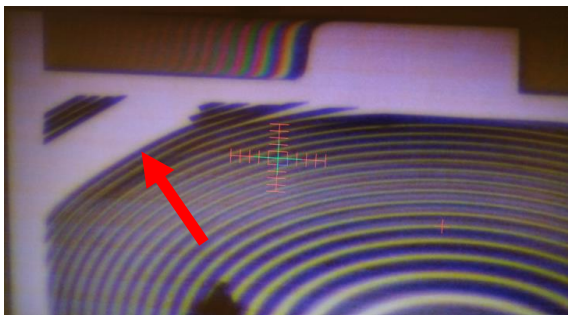

(b)

Figure 24 Diffractive lens (a) after developed good lens, (b) after developed not good lens.

In Figure 24 it shows lens which PR is developed properly; it also shows pattern damage lens after over development.

3.4.3 RIE etching

3.4.3.1 Test structure design

Following the development process, we proceeded with RIE etching using PlasmaPro 100 Estrelas DRIE machine from Oxford instruments. This particular machine provides the flexibility to employ a variety of gas flows; however, for our experiments, we exclusively used three gases: SF6, CHF3, and O_2. To determine the etching rate, test wafer was employed, and we systematically altered different parameters, including Bias power, plasma power, flow rates of SF6, CHF3, and O_2. It's important to note that we maintained the ICP (Inductively Coupled Plasma) power, RF (Radio Frequency) power, temperature, and pressure constants throughout the experiments, with values of 500W, 150W, 10°C, and 10 mTorr, respectively. Initially, we exclusively utilized SF6 gases, as indicated in Table 10.

Table 10 RIE etching rate w. r. t. SF6 flow rate.

No.	SF6 (sccm)	Si Etching depth (µm)	PR Etching depth (µm)	Si etch rate (µm/min)	PR etch rate (µm/min)	Selectivity (PR:Si)
1	1.0	0.77	0.59	0.15	0.12	1:1.31
2	2.0	0.99	0.62	0.20	0.12	1:1.59
3	2.5	1.42	0.79	0.28	0.16	1:1.80
4	3.0	1.42	0.77	0.28	0.15	1:1.85
5	3.5	1.80	0.88	0.36	0.18	1:2.05

Only employing SF6 gas, we observed that both silicon and the PR experienced etching as shown in Figure 26.

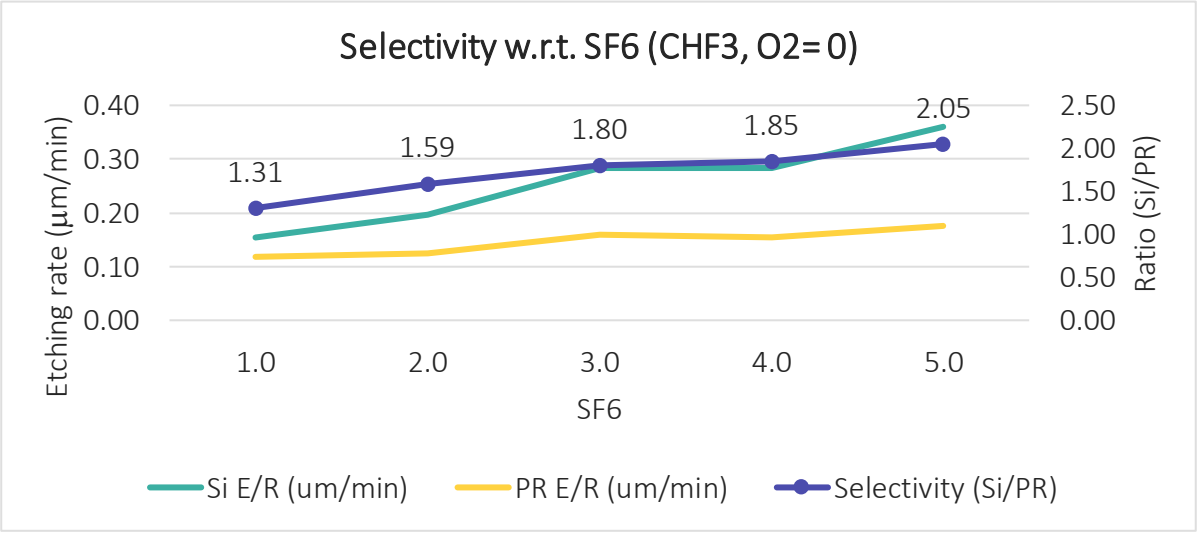

Figure 25 Selectivity graph w. r. t. flow rates of only SF6

The graphical view of the etching process as shown in Figure 26.

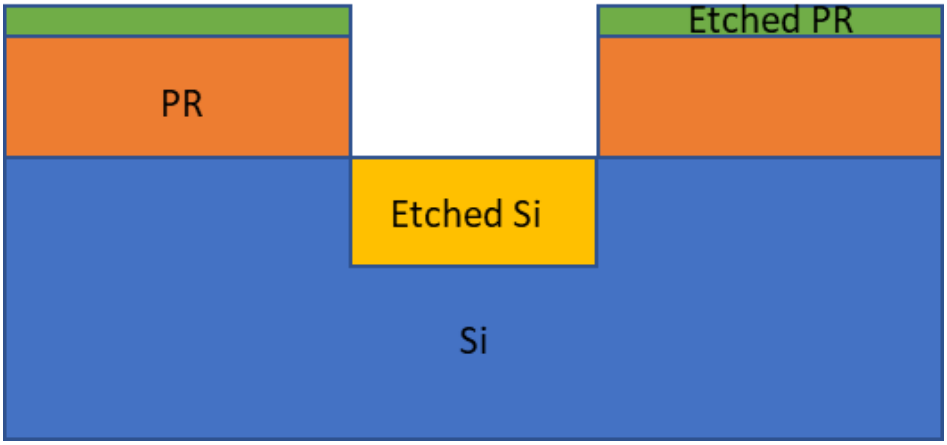

Figure 26 Etching test structure.

However, it's important to note that the etching ratio for Si was notably higher, and this ratio gradually increased with the higher concentration of SF6 gas. A similar trend was observed in the case of PR.

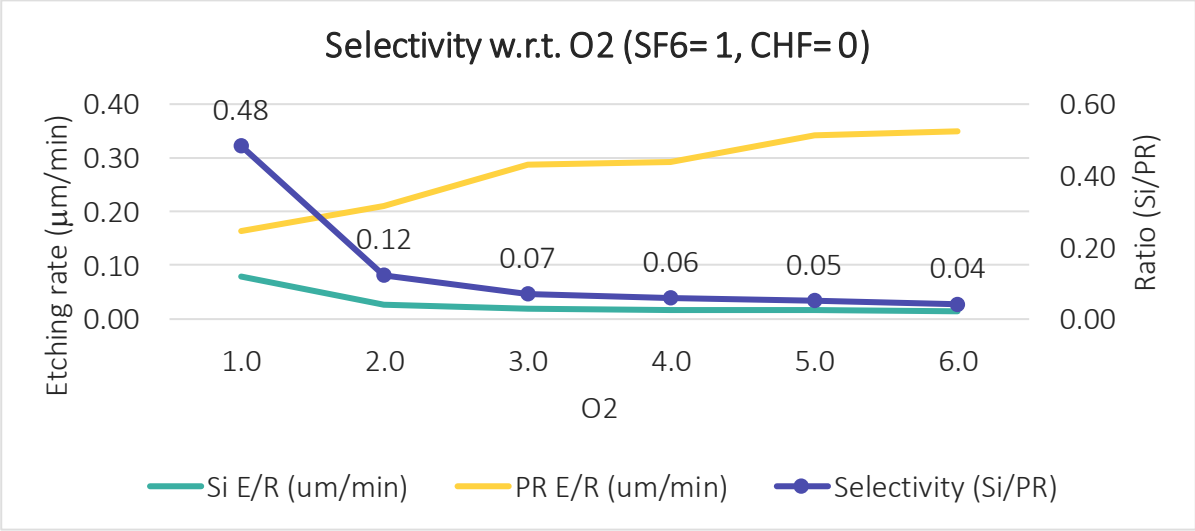

Figure 27 Selectivity graph w. r. t. flow rates of SF6 & O_2

Also, we assessed the etching rate of both silicon and the PR using a constant SF6 flow and varying O_2 flow, ranging from 1 to 6 sccm as shown Figure 27. It was observed that as the O_2 flow increased, the etching rate of PR also increased, while the etching rate of Si decreased. The gas flow remained relatively low and exhibited minor variations. A similar experiment

was conducted by increasing the SF6 flow rate values from 1 to 1.5 and 3 as shown in Figure 28, and Figure 29.

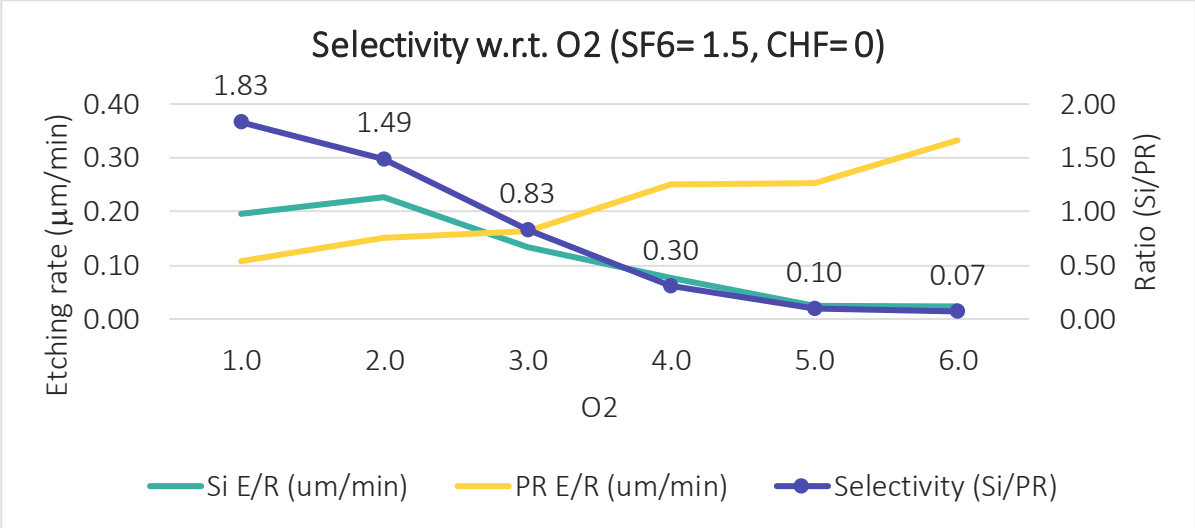

Figure 28 Selectivity w. r. t. SF6 & O_2

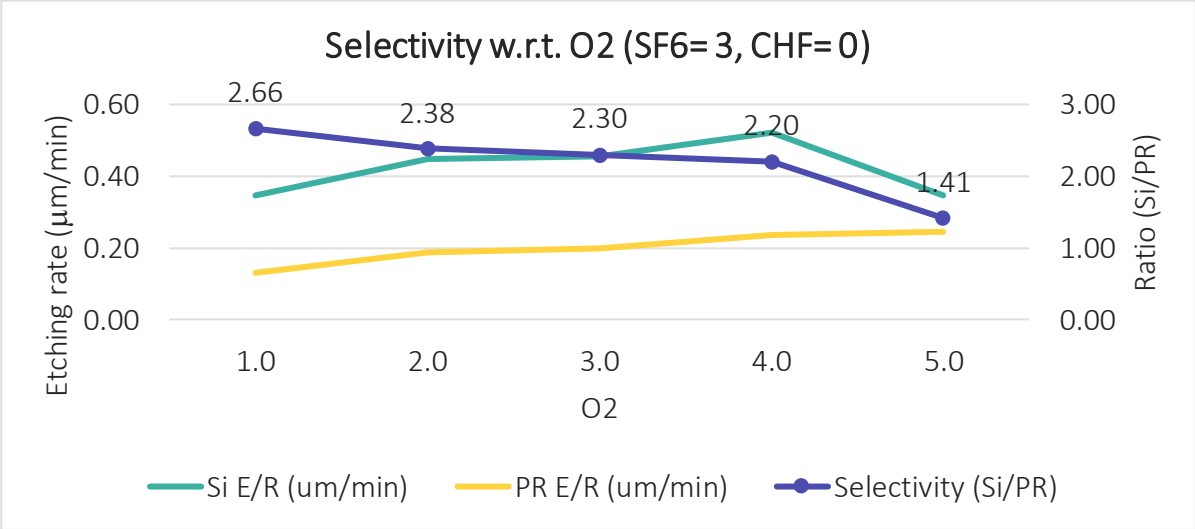

Figure 29 Selectivity w. r. t. flow rates of SF6 & O_2

We can see from both graphs that the Si etching rate exhibits an upward trend with the increasing presence of SF6 and O_2 gases. Conversely, the etching rate of the PR remains relatively consistent across different SF6 values, suggesting that PR etching is more influenced by variations in O_2 and less affected by changes in SF6 concentrations.

Following this observation, we proceeded to investigate the impact of CHF3 gas while keeping SF6 at a constant value. During this particular experiment, O_2 was not introduced, and SF6 remained fixed at 3 sccm, while CHF3 gas flow rates ranged from 10 to 40 sccm as shown in Figure 30.

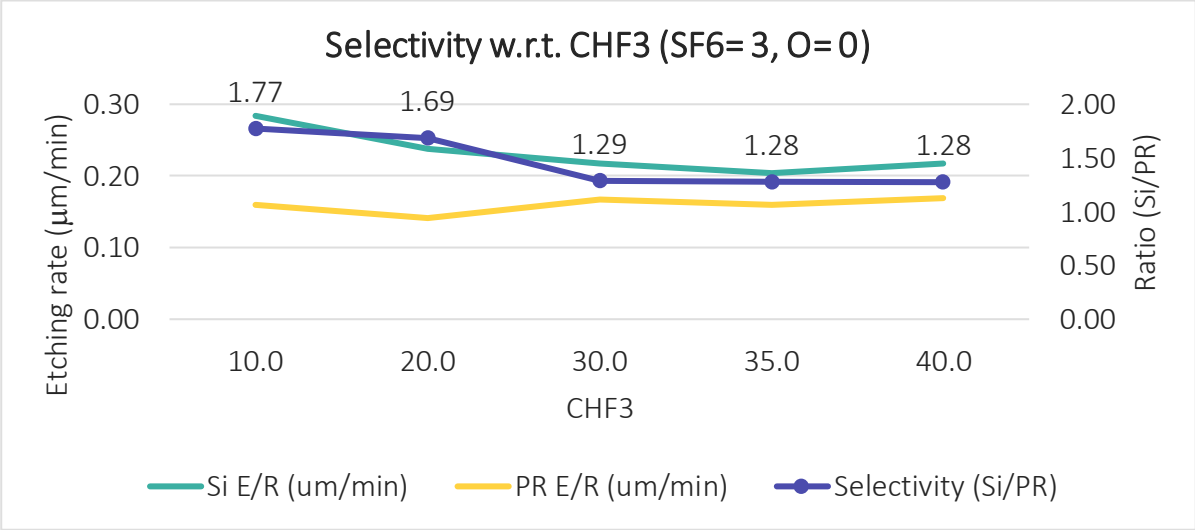

Figure 30 Selectivity w. r. t. flow rates of SF6 & CHF3

Our observations revealed that the introduction of additional CHF3 gas resulted in an increase in silicon etching rates, whereas the etching rate of the PR decreased. Notably, this experiment yielded a selectivity value close to 1, which is significant with implications for diffractive lens design and the overall etching process.

To assess the surface smoothness, we conducted a thorough examination of the surface condition using an optical interferometer as Figure 31. This step aimed to ensure the quality and uniformity of the surface for further applications.

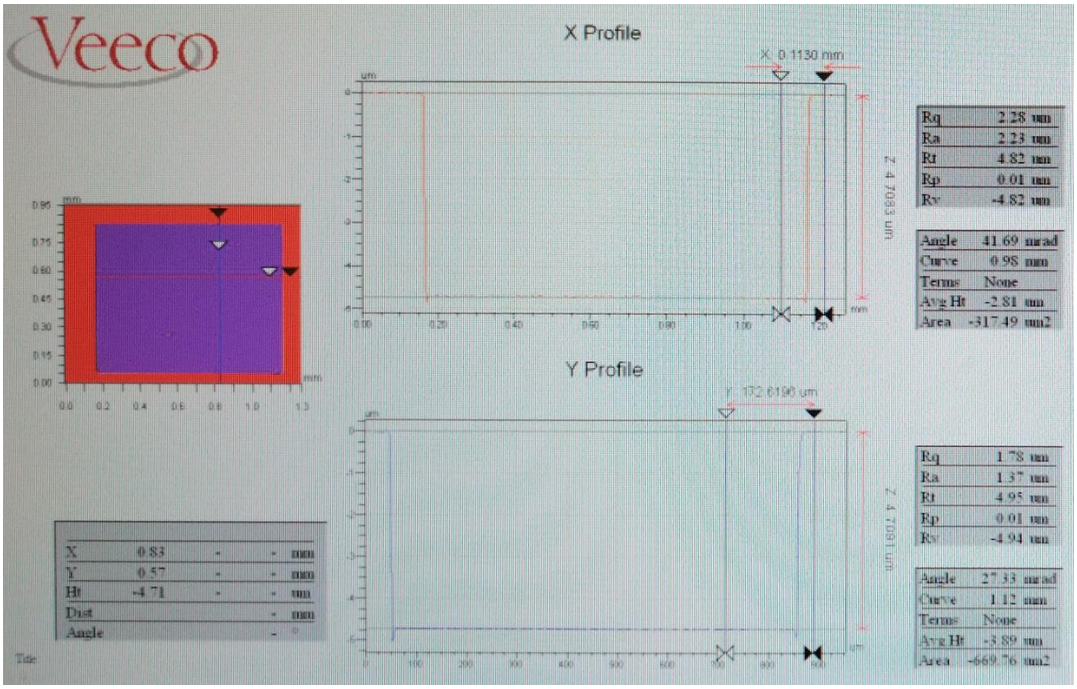

Figure 31 Interferometer data for surface check

3.4.3.2 Diffractive lens fabrication

The optimized recipe derived from the test structure was employed in the etching of the diffractive lens. For this process, we exclusively utilized two gases, SF6 and CHF3, as they demonstrated notably favorable outcomes in terms of etching efficiency and results are shown in Table 11.

Table 11 Diffractive lens RIE etching at various time intervals.

No.	SF6 (sccm)	CHF3 (sccm)	RIE Time (min)	Si Etching depth(µm)	PR Etching depth(µm)	Si etch rate (µm/min)	PR etch rate (µm/min)	Ratio (Si/PR)	Selectivity (PR:Si)
1	3	20	10	Didn't etch on Si due to less etching time					
2	3	20	20						
3	3	20	30	6.33	3.22	0.21	0.11	1.97	1:1.97

This recipe allowed us to achieve a 4π phase profile in the substrate as shown in Figure 32.

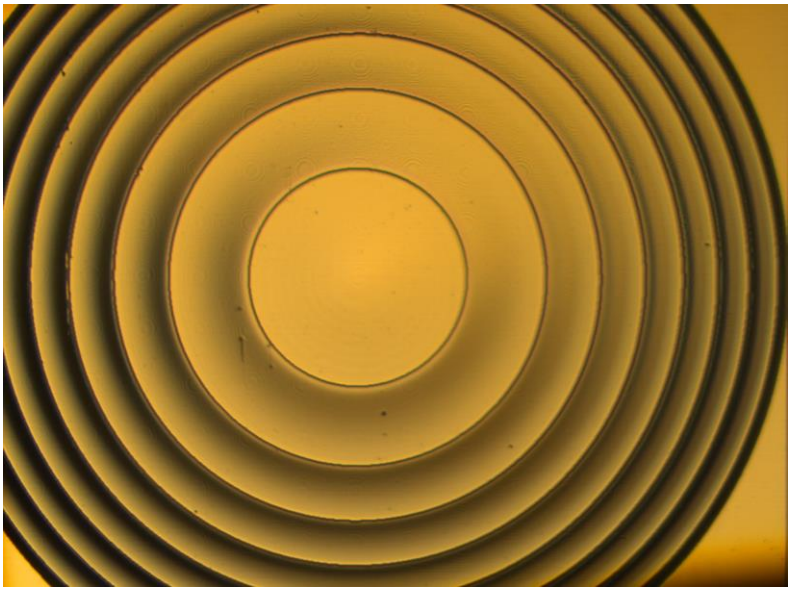

Figure 32 Diffractive lens after RIE, 4π phase profile

Examine the lens condition and closely analyze silicon (Si) etching variations through Scanning Electron Microscope (SEM) images, as shown in Figure 33. The observed images reveal subtle, linear, and smooth vertical changes, forming a grating pattern.

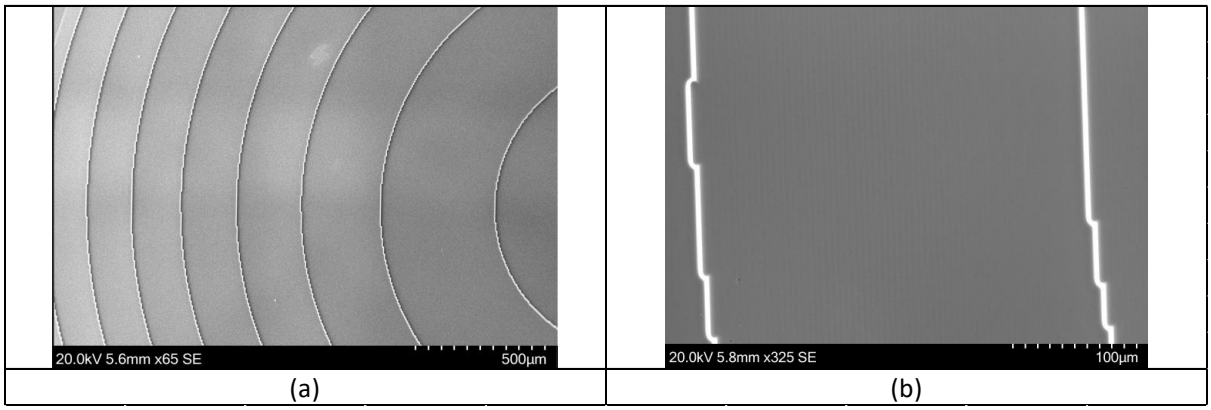

Figure 33 4π phase profile lens SEM picture (a)500um zoom (b)100um zoom picture.

Another recipe for achieving Selectivity of 1 we used to be:

Table 12 Measurement and selectivity 1 data after RIE

Contents	Measurements (μm)			
Exposure energy	250 mJ/cm^2			
Maximum Power	200 μW			
Measurements points	1	2	3	4
PR thickness (μm)	3.79			
After lithography (μm)	3.3	1.16	3.31	2.14
After RIE (SF6= 3, CHF3= 40) (μm)	3.292	1.047	3.465	2.145
Si etched (μm)	3.322	1.098	3.456	2.201
PR etched (μm)	3.33	1.21	3.3	2.2
Selectivity Si/PR	0.997	0.908	1.048	1.001
Selectivity PR:Si	01 : 0.997	01 : 0.908	01 : 1.048	01 : 1.001

By setting the SF6 flow rate to 3 sccm and the CHF3 flow rate to 40 sccm as shown in Table 12, and running the process for 30 minutes, we were able to achieve a selectivity of 1. Our measurements were conducted at four different points, as illustrated in the Figure 22, and demonstrated uniformity across all these points.

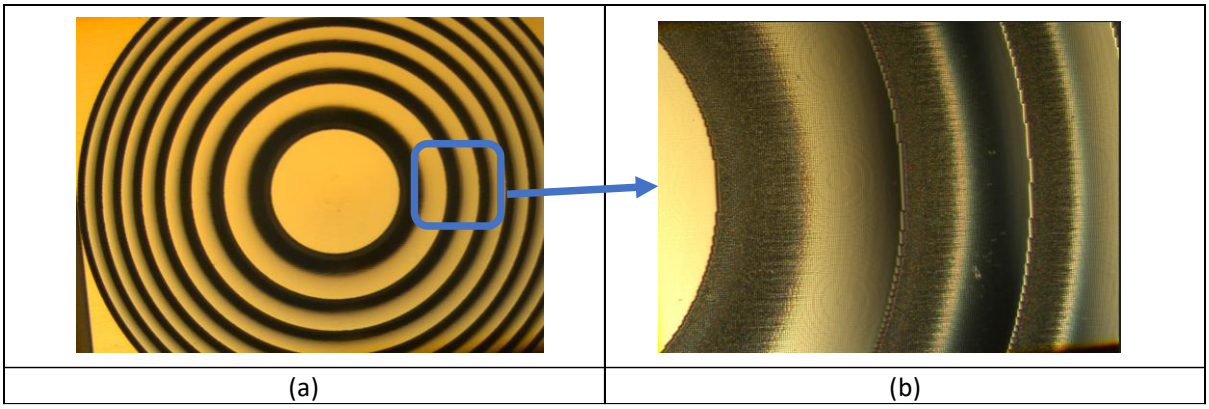

Figure 34 Diffractive lens with selectivity 1 (a) normal view (b) zoom view

Figure 34 are the microscopic picture of the pattern and there is uniformity and grayscale pattern.

Additionally, the etching condition and surface characteristics were checked using SEM, as illustrated in Figure 35.

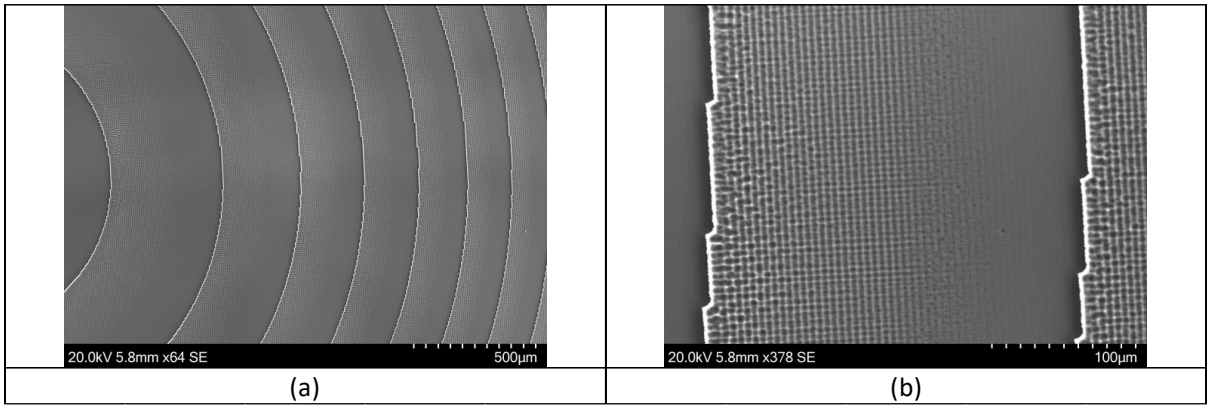

Figure 35 2π phase profile lens SEM picture (a)500um zoom (b)100um zoom picture.

In Figure 33 and Figure 35, variations in lens depth and depth conditions were observed. Figure 33 specifically demonstrates changes in depth conditions characterized by small vertical lines patterns, while in contrast, Figure 35 exhibits Si depth changes with variations in small square patterns.

4 Results

In this research, we conducted a comprehensive analysis of various factors using two distinct processes and different structures. The analysis began with the test structure, where we examined the PR coating process and development, followed by an in-depth investigation into the reactive ion etching (RIE) process, leading to the optimization of RIE and an enhanced understanding of the characteristics of various etching gases.

In the context of the diffractive lens fabrication process, we encountered unique challenges due to the critical and sensitive nature of the structures involved. Unlike binary processes, standard PR development procedures could not be directly applied, necessitating a careful examination of each wafer. The precise timing of the PR development step proved to be of primary importance, as insufficient development time failed to create the desired structures depth, while overdevelopment risked damage to the complex and micro features.

In the test structure design, increasing the concentration of SF6 led to higher etching rates for both silicon (Si) and the PR, with Si exhibiting a faster etching rate than the PR. A similar

trend was observed when O2 was introduced, resulting in an increased PR etching rate, surpassing that of Si. For these experiments, SF6 was used at flow rates ranging from 1 to 3 sccm, and O2 was varied from 1 to 6 sccm. In both cases, we observed a linear relationship between etching rate and selectivity.

Moreover, in experiments involving CHF3 with SF6, and without using O2, the etching selectivity approached 1, demonstrating a high level of consistency. The SF6 flow remained constant at 3 sccm, while CHF3 was adjusted between 10 and 40 sccm. Higher CHF3 flow rates provided more accurate and closer-to-1 selectivity values. These findings highlight the critical role of specific gas combinations and their flow rates in achieving precise etching results.

Subsequent to the optimization of the development process, the RIE process required careful calibration. The test lens experiments helped reveal the notable difference between binary and grayscale RIE processes, providing valuable insights into etching rates and gas combinations for grayscale RIE. Achieving a 4π phase profile height entailed reducing the CHF3 gas flow to approximately 20 sccm, while obtaining an identical phase profile as PR necessitated doubling the CHF3 gas flow to around 40 sccm, ultimately resulting in the achievement of a selectivity of 1.

5 Discussion

5.1 Comparative analysis

Grayscale lithography stands out as an exceptionally versatile and precise technique in contrast to other methods. It excels in creating micro 3D structures, proving highly advantageous for applications in microelectronics, micro-optics, and fabrication. The Pico Master DWL empowers the design and creation of precise structures on PR with micrometer-level depth control, which is impossible with binary lithography. Other grayscale techniques, such as grayscale mask, electron beam lithography, or multi-step exposure, are comparatively more complex and difficult processes when compared to the maskless direct laser writer approach. However, it's worth noting that the maskless DWL process may require

extended durations to produce larger-sized patterns, making it less ideal for mass production scenarios.

5.2 Challenges and limitation

While it was successfully optimized for most of the processes, but RIE process presented unique challenges. RIE machines are exceptionally sensitive, with numerous parameters and gas flows subject to constant but it has variations (±1 sccm) that cannot be completely fixed. The PlasmaPro 100, used for deep etching and Bosch processes to achieve large structures and deeper depths, requires consistent gas flow, but maintaining such micro and complex structure can be challenging. Consequently, any changes in the PR necessitated re-optimization of the PR coating and RIE etching. Despite these challenges, the data obtained from such experiments proved invaluable for future research. It's essential to acknowledge that this optimization's effectiveness is dependent on the specific type and thickness of the PR. Additionally, different RIE etching machines exhibit distinct parameters and effects. Therefore, the results and findings of this study are based on a specific PR and machine and may not be directly applicable to other variations.

6 Conclusion

This research focused on the design and optimization of diffractive lenses fabrication using a maskless grayscale direct laser writer and RIE etching. The primary goal was to achieve a selectivity of 1, a challenging task due to the sensitivity of the RIE etching process such as gas flow rates and other parameters. While 3D structures could be crafted using costly and intricate electron beam lithography, our use of a maskless laser writer provided a cost-effective and efficient solution. Various combinations of gas flows were employed in RIE to comprehend the gas effects on silicon (Si) and photoresist (PR), ultimately achieving a selectivity of up to 2. The accomplishments are outlined as follows:

- A comprehensive discussion and development of the entire lens fabrication process using maskless laser writer grayscale lithography.

- Achievement of selectivities ranging from 1 to 2 by controlling photolithography, development, and RIE etching.
- The utilization of a test Structure aiding in process comprehension and optimization.
- Creation of complex 3D structures with a 4-micrometer thickness of PR.

Diffractive lenses hold versatile applications in both experimental and commercial systems. The expansion of light use extends beyond illumination and communication, encompassing applications such as imaging and sensing also can be effectively applied in imaging systems like cameras, telescopes, and microscopy.

Furthermore, extensive research in PR coating and RIE etching is rare. The results from these combined studies underscore the advantages of grayscale lithography over conventional binary lithography, highlighting the former's flexibility, ease of use, and utility in creating complex 3D structures.

6.1 Future research

This study relied on a single type of PR with a consistent thickness. Future research should encompass a broader range of PRs with varying characteristics, as different PRs have distinct behaviors during development and RIE etching.

To gain a comprehensive understanding of the effects of thickness on the process, further investigation is warranted using PRs of different thicknesses.

As the RIE machine plays a significant role in the lens fabrication process, in-depth studies comparing machine parameters to actual requirements are essential. This research area holds great potential for future exploration.

We can also explore how fine features (narrowest grating or patterns) we can etch using the PicoMaster and RIE.

References

[1] ‘Diffraction Occurs When Wave Passes Edge Stock Vector (Royalty Free) 369964910’, Shutterstock. Accessed: Nov. 03, 2023. [Online]. Available: https://www.shutterstock.com/image-vector/diffraction-occurs-when-wave-passes-edge-369964910

[2] ‘Molecular Expressions: Science, Optics, and You: Light and Color - Diffraction of Light’. Accessed: Oct. 18, 2023. [Online]. Available: https://micro.magnet.fsu.edu/optics/lightandcolor/diffraction.html

[3] A. Vijayakumar and S. Bhattacharya, *Design and Fabrication of Diffractive Optical Elements with MATLAB*. SPIE, 2017. doi: 10.1117/3.2261461.

[4] D. C. O’Shea and Society of Photo-optical Instrumentation Engineers, Eds., *Diffractive optics: design, fabrication, and test*. in Tutorial texts in optical engineering, no. v. TT 62. Bellingham, Wash: SPIE Press, 2004.

[5] J. W. Goodman, *Introduction to Fourier optics*, Fourth edition. New York: W.H. Freeman, Macmillan Learning, 2017.

[6] J. R. Leger, D. Chen, and Z. Wang, ‘Diffractive optical element for mode shaping of a Nd:YAG laser’, *Opt. Lett.*, vol. 19, no. 2, p. 108, Jan. 1994, doi: 10.1364/OL.19.000108.

[7] A. Grushina, ‘Direct-write grayscale lithography’, *Advanced Optical Technologies*, vol. 8, no. 3–4, pp. 163–169, Jun. 2019, doi: 10.1515/aot-2019-0024.

[8] K. Mori, A. Miyazaki, H. Ogasawara, T. Nakamura, and Y. Takeuchi, ‘Numerical Analysis of Sound Pressure Fields Focused by Phase Continuous Fresnel Lens Using Finite Difference Time Domain Method’, *Jpn. J. Appl. Phys.*, vol. 46, no. 7B, pp. 4990–4997, Jul. 2007, doi: 10.1143/JJAP.46.4990.

[9] A. Gürtler, J. J. Gilijamse, A. A. R. Wetzels, L. D. Noordam, E. Sali, and M. Bellini, ‘Frequency selection of supercontinuum ultrashort pulses using a Fresnel zone plate’, *Optics*

Communications, vol. 270, no. 2, pp. 336–339, Feb. 2007, doi: 10.1016/j.optcom.2006.09.029.

[10] V. D. Rumyantsev, 'Solar concentrator modules with silicone-on-glass Fresnel lens panels and multijunction cells', *Opt. Express*, vol. 18, no. S1, p. A17, Apr. 2010, doi: 10.1364/OE.18.000A17.

[11] L. Zhao, W. Duan, and S. F. Yelin, 'All-optical Fresnel lens in coherent media: controlling image with image', *Opt. Express*, vol. 19, no. 2, p. 981, Jan. 2011, doi: 10.1364/OE.19.000981.

[12] M. Amiri and M. T. Tavassoly, 'Fresnel diffraction from 1D and 2D phase steps in reflection and transmission modes', *Optics Communications*, vol. 272, no. 2, pp. 349–361, Apr. 2007, doi: 10.1016/j.optcom.2006.11.048.

[13] J. Kim, D. C. Joy, and S.-Y. Lee, 'Controlling resist thickness and etch depth for fabrication of 3D structures in electron-beam grayscale lithography', *Microelectronic Engineering*, vol. 84, no. 12, pp. 2859–2864, Dec. 2007, doi: 10.1016/j.mee.2007.02.015.

[14] S. Franssila, *Introduction to microfabrication*. Hoboken, N.J.: Wiley, 2013.

[15] J. Chung and W. Hsu, 'Enhancement on forming complex three dimensional microstructures by a double-side multiple partial exposure method', *Journal of Vacuum Science & Technology B: Microelectronics and Nanometer Structures Processing, Measurement, and Phenomena*, vol. 25, no. 5, pp. 1671–1678, Sep. 2007, doi: 10.1116/1.2781527.

[16] K. Totsu, K. Fujishiro, S. Tanaka, and M. Esashi, 'Fabrication of three-dimensional microstructure using maskless gray-scale lithography', *Sensors and Actuators A: Physical*, vol. 130–131, pp. 387–392, Aug. 2006, doi: 10.1016/j.sna.2005.12.008.

[17] C. M. Waits, B. Morgan, M. Kastantin, and R. Ghodssi, 'Microfabrication of 3D silicon MEMS structures using gray-scale lithography and deep reactive ion etching', *Sensors and*

Actuators A: Physical, vol. 119, no. 1, pp. 245–253, Mar. 2005, doi: 10.1016/j.sna.2004.03.024.

[18] I. Khazi, U. Muthiah, and U. Mescheder, '3D free forms in c-Si via grayscale lithography and RIE', *Microelectronic Engineering*, vol. 193, pp. 34–40, Jun. 2018, doi: 10.1016/j.mee.2018.02.006.

[19] S. Deng, Y. Zhang, S. Jiang, and M. Lu, 'Fabrication of three-dimensional silicon structure with smooth curved surfaces', *J. Micro/Nanolith. MEMS MOEMS*, vol. 15, no. 3, p. 034503, Aug. 2016, doi: 10.1117/1.JMM.15.3.034503.

[20] T. Nachmias, A. Ohayon, S. E. Meltzer, M. Kabla, E. Louzon, and U. Levy, 'Shallow Fresnel lens fabrication using grayscale lithography made by high energy beam sensitive mask (HEBS) technology and reactive ion etching', presented at the SPIE MOEMS-MEMS: Micro- and Nanofabrication, T. J. Suleski, W. V. Schoenfeld, and J. J. Wang, Eds., San Jose, CA, Feb. 2009, p. 72050B. doi: 10.1117/12.809376.

[21] C. McKenna, K. Walsh, M. Crain, and J. Lake, 'Maskless Direct Write Grayscale Lithography for MEMS Applications', in *2010 18th Biennial University/Government/Industry Micro/Nano Symposium*, Jun. 2010, pp. 1–4. doi: 10.1109/UGIM.2010.5508906.

[22] S. G. BV, 'SPIN150i-NPP Single Substrate Spin Processor', www.sps-international.com. Accessed: Oct. 29, 2023. [Online]. Available: https://www.sps-international.com/product/spin150i-npp-single-substrate-spin-processor/15876/

[23] 'Direct laser writers | PICOMASTER | Raith', https://raith.com/. Accessed: Oct. 27, 2023. [Online]. Available: https://raith.com/product/picomaster/

[24] 'LIMS - [View Tool]'. Accessed: Oct. 28, 2023. [Online]. Available: http://usn.norfab.no/WebForms/Equipment/EquipmentView.aspx?toolId=8

[25] 'PlasmaPro 100 Estrelas DRIE', Oxford Instruments. Accessed: Oct. 28, 2023. [Online]. Available: https://plasma.oxinst.com/products/dsie/plasmapro-100-estrelas-dsie

[26] ‘ma-P 1200’, Kayaku Advanced Materials, Inc. Accessed: Oct. 28, 2023. [Online]. Available: https://kayakuam.com/products/ma-p-1200/

[27] ‘mr-D 526/S – Microresist’. Accessed: Oct. 29, 2023. [Online]. Available: https://www.microresist.de/en/produkt/mr-d-526-s/

[28] J. A. Jordan, P. M. Hirsch, L. B. Lesem, and D. L. Van Rooy, ‘Kinoform Lenses’, *Appl. Opt.*, vol. 9, no. 8, p. 1883, Aug. 1970, doi: 10.1364/AO.9.001883.

[29] T. R. M. Sales and G. M. Morris, ‘Diffractive–refractive behavior of kinoform lenses’, *Appl. Opt.*, vol. 36, no. 1, p. 253, Jan. 1997, doi: 10.1364/AO.36.000253.

[30] J.-J. Clair, ‘New methods to synthesise kinoforms’, *Optics Communications*, vol. 6, no. 2, pp. 135–137, Oct. 1972, doi: 10.1016/0030-4018(72)90211-8.

List of tables and charts

List of the figures